Experimental Determination of Transfer Functions of Beams and Plates by Cross-Correlation Techniques

By

HAROLD GEORGE KIZNER

A DISSERTATION PRESENTED TO THE GRADUATE COUNCIL OF
THE UNIVERSITY OF FLORIDA
IN PARTIAL FULFILLMENT OF THE REQUIREMENTS FOR THE
DEGREE OF DOCTOR OF PHILOSOPHY

UNIVERSITY OF FLORIDA

June, 1962

ACKNOWLEDGMENTS

The author would like to express his appreciation to Professor William A. Nash, Chairman of his Supervisory Committee, for suggesting the topic of this study and for guidance and encouragement throughout the course of this investigation.

He also wishes to express his appreciation to Dr. T. S. George, Professor of Electrical Engineering, Professor William L. Sawyer, Head of the Department of Engineering Mechanics, Dr. T. C. Huang, Associate Professor of Engineering Mechanics, and Dr. C. B. Smith, Professor of Mathematics, for serving on his Supervisory Committee.

The author is particularly indebted to Miss Eileen Bailey, who painstakingly typed this dissertation.

Finally, the author expresses his appreciation to the Air Force Office of Scientific Research for their sponsorship of the work.

TABLE OF CONTENTS

Page

ACKNOWLEDGMENTS ii

LIST OF TABLES iv

LIST OF FIGURES v

NOMENCLATURE ix

Chapter

I. INTRODUCTION 1

II. APPLICATION OF CORRELATION AND SPECTRAL ANALYSIS TO THE VIBRATION OF ELASTIC SYSTEMS 6

III. THEORETICAL FORMULATION OF THE PROBLEM 14

IV. EXPERIMENTAL INVESTIGATION 19

V. NORMAL MODE DETERMINATION OF THE TRANSFER FUNCTION 45

VI. PRESENTATION AND DISCUSSION OF EXPERIMENTAL RESULTS 64

LIST OF REFERENCES 104

BIOGRAPHICAL SKETCH 106

LIST OF TABLES

Table Page

1. Experimentally Determined Beam Parameters 50

2. Real (R) and Imaginary (I) Parts of the Transfer Function 56

3. Characteristic Mode Shapes for Cantilever Beam . . . 57

4. Coefficients of a_n 58

5. Contribution of the n^{th} Mode to the Transfer Function 62

6. Real and Imaginary Components of the Transfer Function for Acceleration and Displacement 63

LIST OF FIGURES

Figure Page

1. Beam Test Apparatus and Support 20

2. Plate Test Apparatus and Support 21

3. Experimental Flow Chart Showing Arrangement of Equipment 22

4. Recording of Random Pressure from a Subsonic Air Jet 23

5. Oscilloscope Record of Force and Acceleration of Beam 25

6. Oscilloscope Record of Force and Acceleration of Plate 25

7. Autocorrelation of Force at Position 1313 26

8. Structural Feedback Effect on Spectral Density Input 29

9. Flow Diagram for the Evaluation of Correlation . . . 31

10. Cross-Correlation of Force-Acceleration for 0013. . 33

11. Real and Imaginary Parts of Cross-Power Spectral Density of Force-Acceleration for 0011 36

12. Real and Imaginary Parts of Cross-Power Spectral Density of Force-Acceleration for 0012 37

13. Real Part of Cross-Power Spectral Density of Force Acceleration for 0013 38

14. Imaginary Part of Cross-Power Spectral Density of Force Acceleration for 0013 39

LIST OF FIGURES--Continued

Figure Page

15. Power Spectral Density of Input Force 40

16. Autocorrelation of Input Force for Plate at 1313 . . . 41

17. Cross-Correlation of Force-Acceleration for the Plate at 0021 42

18. Cross-Power Spectral Density of Force-Acceleration 43

19. Real Part of Beam Response Represented as a Single Degree-of-Freedom System 47

20. Imaginary Part of Beam Response Represented as a Single Degree-of-Freedom System 48

21. Oscilloscope Record of Beam Transient for Second Mode 52

22. Oscilloscope Record of Beam Transient for Third Mode 52

23. Plot of Logarithmic Decrement for the Second Mode of Vibration 54

24. Modulus of Acceleration Transfer Function at 0011 . 68

25. Modulus of Acceleration Transfer Function at 0012 . 69

26. Modulus of Acceleration Transfer Function at 0013 . 70

27. Modulus of Acceleration Transfer Function at 0014 . 71

28. Modulus of Acceleration Transfer Function at 0015 . 72

29. Modulus of Acceleration Transfer Function at 0016 . 73

LIST OF FIGURES--Continued

Figure Page

30. Modulus of Acceleration Transfer Function at 0017 . . 74

31. Phase Angle of Acceleration Transfer Function at 0011 75

32. Phase Angle of Acceleration Transfer Function at 0012 76

33. Phase Angle of Acceleration Transfer Function at 0013 77

34. Phase Angle of Acceleration Transfer Function at 0014 78

35. Phase Angle of Acceleration Transfer Function at 0015 79

36. Phase Angle of Acceleration Transfer Function at 0016 80

37. Phase Angle of Acceleration Transfer Function at 0017 81

38. Plan View of Plate 82

39. Modulus of Acceleration Transfer Function at 0011 . . 83

40. Modulus of Acceleration Transfer Function at 0012 . . 84

41. Modulus of Acceleration Transfer Function at 0013 . . 85

42. Modulus of Acceleration Transfer Function at 0021 . . 86

43. Modulus of Acceleration Transfer Function at 0022 . . 87

44. Modulus of Acceleration Transfer Function at 0023 . . 88

LIST OF FIGURES--Continued

Figure Page

45. Modulus of Acceleration Transfer Function at 0031 . . 89

46. Modulus of Acceleration Transfer Function at 0032 . . 90

47. Modulus of Acceleration Transfer Function at 0033 . . 91

48. Phase Angle of Acceleration Transfer Function at 0011 92

49. Phase Angle of Acceleration Transfer Function at 0012 93

50. Phase Angle of Acceleration Transfer Function at 0013 94

51. Phase Angle of Acceleration Transfer Function at 0021 95

52. Phase Angle of Acceleration Transfer Function at 0022 96

53. Phase Angle of Acceleration Transfer Function at 0023 97

54. Phase Angle of Acceleration Transfer Function at 0031 98

55. Phase Angle of Acceleration Transfer Function at 0032 99

56. Phase Angle of Acceleration Transfer Function at 0033 100

57. Complete Assembly of Experimental Equipment . . . 103

NOMENCLATURE

b	Coefficient of viscous damping
B	Correlator bandwidth
D	Dimensionless damping factor
$\overline{E}$	Expected value
E	Modulus of elasticity
f	Frequency in cycles per second
f_n	Undamped natural frequency
$f_i(r,t)$	Input as a function of space and time
$f_o(r,t)$	Output as a function of space and time
$H(r,\omega)$	Transfer function or generalized response function
$h(r,t)$	Unit impulse response function
I	Logarithmic decrement
i	Imaginary number, $i = \sqrt{-1}$

k	Equivalent spring constant
ℓ	Length of beam
m	Equivalent mass of structure
M_n	Generalized mass
$p(r,t)$	Lateral force on the structure
$\vec{r}, \vec{s}$	Position vectors on the surface of the structure
dr, ds	Elemental surface area
$R(t_1, t_2)$	Nonstationary autocorrelation
$R_{ii}(s,\tau)$	Autocorrelation of input force $f_i(s,t)$ at point s
$R_{io}(r,s,\tau)$	Cross-correlation of two random space-time functions, $f_i(r,t)$ and $f_o(s,t)$, at positions r and s, respectively
$S(\omega)$	Power spectral density as a function of the angular frequency in radians per second
t	Time
T	Smoothing time or time length of the sample record

$\mu(r,t)$	Lateral displacement of the structure
$V_m(x/\ell)$	Normal mode shape of motion at the position of force
$V_m(\eta/\ell)$	Normal mode shape of motion at the accelerometer position
α	Dimensionless parameter representing the autocorrelation delay τ
β	Dimensionless parameter representing the correlator smoothing time T
β_n	Generalized damping coefficient
γ, δ	Time variables
η	Position of accelerometer
K	Natural frequency for single degree-of-freedom system
λ_m	Natural frequency of the m^{th} mode
ν	Damped circular frequency
σ^2_{xx}	Variance, mean square variation about the mean
$\left(\frac{R}{\sigma}\right)_{out.}$	Signal-to-noise amplitude ratio of the correlator

τ	Time delay
$\Phi_{ii}(r,\omega)$	Power spectral density of the input force $f_i(r,t)$
$\Phi_{io}(r,s,\omega)$	Cross-power spectral density of $f_i(r,t)$ and $f_o(s,t)$, respectively
ω	Angular frequency in radians per second
ω_n	Natural frequency of the nth mode in radians per second
$*$	Denotes complex conjugate

CHAPTER I

INTRODUCTION

One of the criteria for the mechanical design of a structure involves a consideration of the structural response to a discrete frequency vibration excitation. In the case of a random loading, the problem becomes more difficult and time consuming since we now must deal with a continuous spectrum of vibration excitation. Before it is possible to predict the probable response of structures to random loads, one must first define the loading which will probably occur on the structure.

The objective of this study is to experimentally evaluate the transfer function of several structures under stationary environmental conditions. To attain this end, the random pressure from a subsonic air jet has been regarded as a statistically defined load. Once the load has been defined, the problem reduces to the determination of the transfer function and then to the prediction of the probable response.

For the given statistical input, it is possible to measure, on a specimen, the transfer function as a function of frequency for the points of interest. From these measurements on the structure, it will then be possible to ascertain the validity of other theoretical representations of the same structural characteristics.

A common method of analysis makes use of several normal modes of a coupled spring-multiple mass-dashpot system and permits the calculation of the transfer function for these coupled modes of vibration. The larger number of normal modes actually present in the structure may not allow one to consider such a model as describing the measured curve adequately.

A single degree-of-freedom system has for its magnification factor

$$H = \frac{1}{\sqrt{\left[1-\left(f/f_n\right)^2\right]^2+\left[2\zeta\left(f/f_n\right)\right]^2}} \tag{1.1}$$

in which

$f_n = \sqrt{k/m}$

f = the impressed frequency

ζ = critical damping ratio

k = equivalent spring constant

m = mass

The response to an excitation at a particular frequency f_a is

Response = (Excitation at f_a) · (Transfer function at f_a)

$$u_{f_a} = \sqrt{\left(E_{f_a} \cdot H_{f_a}\right)^2} = E_{f_a} \cdot H_{f_a} \tag{1.2}$$

where

E_{f_a} = rms excitation at f_a

H_{f_a} = transfer function at f_a

U_{f_a} = rms response

For several discrete frequency excitations, the rms response is

$$U = \sqrt{\sum_m \left(E_{f_a} \cdot H_{f_m}\right)^2} \tag{1.3}$$

and may be extended to a continuous spectrum of excitation as

$$U = \sqrt{\int_0^\infty \left(E_w \cdot H_w\right)^2 dw} \tag{1.4}$$

where E_w is the power spectral density of the input force. The response of a complex structure vibrating in all its modes could then be evaluated by superposition of the modal responses.

Aside from the fact that the results for several modes may not give an accurate description of the response, the time required to go through the above process is not justifiable. With this in mind, the response function is determined for a nonuniform spectral density input. An experimental program, based on a cross-correlation theorem, is undertaken to determine the transfer function for several structures and in one case is compared with the theoretical modal approach.

It is known that the input-output cross-correlation of a linear system is the convolution of the unit-impulse response and the input autocorrelation. When the effective bandwidth of the input spectral density $\Phi(\omega)$ is not white, i.e., not independent of frequency over a relatively broad frequency interval, it is not an easy matter to obtain the transfer function. The experimental determination of $H(\vec{r},\omega)$ is carried out by working exclusively in the frequency domain. If the input force power spectral density had been white noise, the cross-correlation of the output acceleration with input force would be directly proportional to the unit-impulse response [1].* In a block diagram this is expressed as follows.

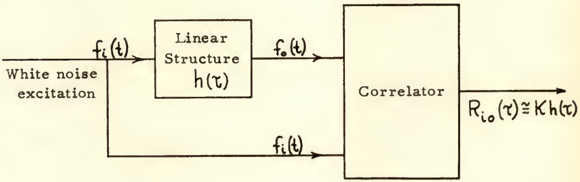

A special purpose correlator was constructed to serve this purpose. The method of cross-correlation has a distinct advantage over other conventional methods for measuring $H(\vec{r},\omega)$ or $h(t)$.

---

[*] The numbers in brackets refer to entries in the List of References.

Instead of applying a step input and recording the response, one can now measure the transfer function under stationary conditions. Thus, for a stationary random input, the input can be regarded as the excitation for the unit-impulse measurement. This is valid if the input noise is flat and wide compared to the bandwidth of the system. The procedure is to measure the cross-correlation $R_{io}(r,s,\tau)$ and $R_{ii}(s,\tau)$ and then to find $H(r,\omega)$ by a spacewise Fourier transformation of $R_{io}(r,s,\tau)$ and $R_{ii}(s,\tau)$. However, considerable computation is necessary to produce results of acceptable accuracy.

CHAPTER II

APPLICATION OF CORRELATION AND SPECTRAL ANALYSIS TO THE VIBRATION OF ELASTIC SYSTEMS

A statistical treatment for any linear structure with known normal modes excited by random forces of given power spectral density of excitation has been carried out. The mean square response can be evaluated, and the probability distribution of the response exceeding an assigned value is then available under the assumption of a Gaussian distribution into the system. The response of these systems has always been determined without inclusion of spacewise effects. They have been studied by Van Lear and Uhlenbeck [2], Eringen [3] and Thompson [4].

The basic philosophy of the treatment of random-in-time phenomena has been given by Rice [5]. The restriction that the noise be a "stationary" process, and furthermore that it be "Gaussian" will be assumed, although the latter assumption is not needed in computing the system response function. The fact that the process is stationary Gaussian allows us to completely specify the process by its correlation function or spectrum. Furthermore, an ensemble whose sample functions are sums of sample functions from Gaussian random processes is, as might be expected from the central limit theorem, the ensemble of a Gaussian process. Thus, the assumption that the physical disturbance of the structure is caused by innumerable random disturbances justifies the assumption that the phenomena be Gaussian. The assumption of a stationary process is important because, otherwise, the statistical properties may change in time.

Only for a linear system is it possible to relate by linear operation certain averages of the output, e.g., the correlation function, spectrum and average power to the correlation function or spectrum of the input process. No more than the spectrum of the input need be known to compute the corresponding quantity for the output process. This does not, by any means, say that the correlation or spectrum describes the output process completely. Unless we assume that the process is Gaussian, the spectrum and correlation provide little insight in determining the probability distribution of the response. For a stationary process the correlation may be written as

$$R(t_1,t_2) = \bar{E}(x_{t_1}, x_{t_2}) = R(t_2-t_1) = R(\tau) \qquad (2.1)$$

since the time average cannot be a function of time and can depend only on time differences. Here, $\bar{E}$ is the ensemble average and R

denotes the covariance or autocorrelation. When we further make the assumption that the process is ergodic, we can also say that

$$R(t_1, t_2) = R(\tau) = \lim_{T\to\infty} \frac{1}{2T} \int_{-T}^{T} x(t)\,x(t+\tau)\,dt \qquad (2.2)$$

In the above we have interchanged an ensemble average for a time average.

It should be mentioned that the well-established techniques of spectral analysis developed by Rice [5] are not in general applicable to nonlinear systems, although the analysis can be extended to cover systems containing small nonlinearity [6]. A structure with nonlinear damping, for instance, would not theoretically permit us to employ the concepts of linear harmonic analysis to analyze its response and would consequently require the determination of the probability density function.

The basic relation that determines the response, u , of a beam or plate is the following differential equation:

$$m\ddot{u} + b\dot{u} + L(u) = p(\vec{r}, t) \qquad (2.3)$$

where L is the appropriate differential operator, b is the coefficient of viscous damping and p denotes the forcing function. For the plate the operator, L , is

$$L = C\left(\frac{\partial^2}{\partial x^2} + \frac{\partial^2}{\partial y^2}\right)^2 \tag{2.4}$$

where C is a constant depending on the velocity of wave propagation and the properties of the plate.

In an eigenvalue approach we consider solutions of the Sturm-Liouville equation

$$m\ddot{\mu} + L\left(\mu\right) = 0 \tag{2.5}$$

satisfying the relevant boundary conditions. The normal mode solutions are taken in the form

$$\mu_n = V_n(\vec{r})\ e^{i\omega_{o_n} t} \tag{2.6}$$

where ω_{o_n} is the natural circular frequency of the n^{th} mode whose shape is given by the corresponding $V_n(\vec{r})$. The solution to the original differential equation can be assumed to take the form

$$\mu = \sum_n V_n(\vec{r})\, f_n(t) \tag{2.7}$$

Substituting (2.6) into (2.5) gives

$$-m\omega_{o_n}^2 V_n(\vec{r}) + L\left[V_n(\vec{r})\right] = 0 \tag{2.8}$$

The solution of (2.3), using (2.7) and (2.8), becomes

$$m\sum_n V_n(\vec{r})\ddot{f}_n(t) + b\sum_n V_n(\vec{r})\dot{f}_n(t) + \sum_n m\omega_{o_n}^2 V_n(\vec{r}) = p(\vec{r},t) \tag{2.9}$$

We next use the orthogonality property of normal modes, i.e.,

$$\int_{\vec{r}} V_n(\vec{r})\ V_m(\vec{r})\, d\vec{r} = 0\ , \qquad m \neq n \tag{2.10}$$

and for $m = n$

$$M_n = \int m V_n^2(\vec{r})\, d\vec{r} \tag{2.11}$$

where M_n denotes the generalized mass, and assume that there is no damping coupling between modes, i.e.,

$$\int b V_n(\vec{r})\ V_m(\vec{r})\, d\vec{r} = 0 \qquad m \neq n \tag{2.12}$$

and

$$\beta_n = \frac{1}{M_n} \int b V_n^2(\vec{r})\, d\vec{r}\ , \tag{2.13}$$

where β_n is a generalized damping coefficient (1/sec).

On multiplying equation (2.9) by $V_m(\vec{r})$ and integrating over the area, this equation becomes

$$\ddot{f}_n(t) + \beta_n \dot{f}_n(t) + \omega_{o_n}^2 f_n(t) = \frac{1}{M_n} \int p(\vec{r},t)\, V_n(\vec{r})\, d\vec{r} \tag{2.14}$$

Taking the Fourier transform of the random input pressure as

$$\Phi_p(\vec{r},\omega) = \frac{1}{\sqrt{2\pi}} \int_{\infty}^{\infty} p(\vec{r},t)\, e^{-i\omega t}\, dt \tag{2.15}$$

and the output $f_n(\vec{r},t)$ as

$$\Phi_{f_n}(\omega) = \frac{1}{\sqrt{2\pi}} \int_{\infty}^{\infty} f_n(t)\, e^{-i\omega t}\, dt \tag{2.16}$$

equation (2.14) can be transformed to

$$\left(-\omega^2 + i\beta_n\omega + \omega_{o_n}^2\right) \Phi_{f_n}(\omega) = \frac{1}{M_n} \int \Phi_p(\vec{r},\omega) V_n(\vec{r})\, d\vec{r} \tag{2.17}$$

where ω_{o_n} is the natural frequency of the nth mode.

To introduce the power spectral density, we assume that the process is ergodic, which allows us to write the spectral density, $S_\mu(\omega)$, of a single function from the ensemble, i.e.,

$$S_\mu(\vec{r},\omega) = \frac{2}{T}\, \Phi(\vec{r},\omega)\, \Phi^*(\vec{r},\omega) \tag{2.18}$$

the asterisk indicating the complex conjugate. Substitution into equation (2.17) gives the output power spectrum in terms of the input spectrum, viz.,

$$S_{\mu}(\vec{r},s,\omega)=\sum_{n}\sum_{m}\frac{V_n(\vec{r})\,V_m(\vec{r})}{H_n(\omega)\,H_m(\omega)}\iint\frac{2}{T}S_p(\vec{r},\omega)\,S_p^{*}(\vec{r},\omega)\,e^{-i(\theta_n-\theta_m)}\,V_n(\vec{r})\,V_m(\vec{r})\,d\vec{A} \qquad (2.19)$$

where

$$\left|H_{n}\cancel{(n}(\omega)\right|^{2} = M_n^{2}\left[\left(\omega_n^{2}-\omega^{2}\right)^{2}+\beta_n^{2}\omega^{2}\right] \qquad (2.20)$$

and

$$\tan\,\theta = \frac{\beta_n\omega}{(\omega_n^{2}-\omega)} \qquad (2.21)$$

For the case of a rectangular plate, equation (2.19) can be put in another form [7],

$$S_{\mu}(r,s,\omega) = \sum_{n}\sum_{m}\frac{V_n(r)\,V_m(r)}{b_m\,b_n(\lambda_m^{2}-\omega^{2}-2i\beta_m\omega)(\lambda_n^{2}-\omega^{2}+2i\beta_n\omega)}\cdot\iint V_n(s)\,V_m(s)\,S_p(r,s,\omega)\,dA \qquad (2.22)$$

$$n = 1,2,\ldots\ldots$$
$$m = 1,2,\ldots\ldots$$

where b_m is a generalized length for a beam and a generalized area for a plate, and the λ_m represent eigenvalues.

The term under the double summation sign represents the transfer function as a function of space and frequency. In a subsequent chapter this term is specialized for the case of a beam by deleting one of the space dimensions and then summing with respect to five modes.

CHAPTER III

THEORETICAL FORMULATION OF THE PROBLEM

The purpose of this study was to attempt to apply the methods of communication theory to an analysis of the response function of structures subjected to a loading which is a function of space as well as of time. The derivation of the cross-correlation theorem follows and is then applied to the determination of the characteristics of a linear system.

In a linear system subject to a random force input, the relation between the input force autocorrelation and output autocorrelation (of either displacement, velocity or acceleration) is

$$R_{oo}(r,s,\tau) = \int_{-\infty}^{\infty} h(r,s,\gamma)\,d\gamma \int_{-\infty}^{\infty} h(r,s,\delta)\,R_{ii}(r,s,\tau+\gamma-\delta)\,d^3s\,d\delta \qquad (3.1)$$

where $d^3s = dx_i\,dy_i\,dz_i$ and the integration is extended over the entire region of the structure. Here γ and δ are dummy time variables.

This relation is found by using the definitions of input and output autocorrelation functions and then applying the convolution integral,

$$f_o(r,t) = \int_{-\infty}^{\infty} h(r,s,\gamma) f_i(s,t-\gamma) d^3s\, d\gamma \tag{3.2}$$

where the integration is extended over the region defined by the input. Equation (3.1) could be further developed in order to obtain the unit impulse response, $h(r,s,\tau)$, but since it appears under the integral sign, its evaluation is difficult. The unit impulse response, or Green's function, is more readily evaluated by considering the following cross-correlation theorem and then expressing it in the frequency domain.

For a linear structure a theorem exists involving the input-output cross-correlation, the input autocorrelation, and the unit-impulse response, $h(r,\tau)$ [8]. The theorem is obtained by starting with the definition of the input-output cross-correlation $R_{io}(r,s,\tau)$

$$R_{io}(r,s,\tau) = \lim_{T\to\infty} \frac{1}{2T} \int f_i(r,t)\, f_o(s,t+\tau)\, dt \tag{3.3}$$

In order to introduce $h(r,t)$ into this expression, we make use of the convolution integral for $f_o(r, t+\tau)$. Thus,

$$R_{io}(r,s,\tau) = \lim_{T\to\infty} \frac{1}{2T} \int_{-T}^{T} f_i(r,t) \int_{-\infty}^{\infty} h(r,s,\gamma) f_i(s,t+\tau-\gamma) d^3s\, d\gamma\, dt \tag{3.4}$$

where $f_i(r,t)$ is a scalar force field defined at every point in space. Inverting the order of integration, we have

$$R_{io}(r,s,\tau) = \int_{-\infty}^{\infty} h(r,s,\gamma)\, d\gamma \lim_{T\to\infty} \frac{1}{2T} \int_{-T}^{T} f_i(r,t)\, f_i(s,t+\tau-\gamma)\, d^3s\, dt \qquad (3.5)$$

Since

$$R_{ii}(r,\tau-\gamma) = \lim_{T\to\infty} \frac{1}{2T} \int_{-\infty}^{\infty} f_i(r,t)\, f_i(s,t+\tau-\gamma)\, d^3s\, dt \qquad (3.6)$$

equation (3.5) becomes

$$R_{io}(r,s,\tau) = \int_{-\infty}^{\infty} h(r,s,\gamma)\, R_{ii}(r,\tau-\gamma)\, d\gamma \qquad (3.7)$$

This is the statement that relates the input-output cross-correlation of a linear system through the convolution of the unit-impulse response and the input autocorrelation.

To express this in the frequency domain, we take the Fourier transform of both sides of the equation, viz.,

$$\frac{1}{2\pi} \int_{-\infty}^{\infty} R_{io}(r,s,\tau)\, e^{-i\omega\tau}\, d\tau = \frac{1}{2\pi} \int_{-\infty}^{\infty} e^{-i\omega\tau}\, d\tau \int_{-\infty}^{\infty} h(r,s,\gamma)\, R_{ii}(r,\tau-\gamma)\, d\gamma \qquad (3.8)$$

Introducing the Fourier transform pairs

$$\Phi_{io}(r,\omega) = \frac{1}{2\pi}\int_{-\infty}^{\infty} R_{io}(r,\tau)\, e^{-i\omega\tau}\, d\tau \tag{3.9}$$

$$H(r,s,\omega) = \int_{-\infty}^{\infty} h(r,s,\tau)\, e^{-i\omega\tau}\, d\tau \tag{3.10}$$

$$\Phi_{ii}(r,\omega) = \frac{1}{2\pi}\int_{-\infty}^{\infty} R_{ii}(r,\tau)\, e^{-i\omega\tau}\, d\tau \tag{3.11}$$

and letting $\delta = \tau - \gamma$

$$\Phi_{io}(r,s,\omega) = \frac{1}{2\pi}\int_{-\infty}^{\infty} e^{-i\omega(\delta+\gamma)}\, d\delta \int_{-\infty}^{\infty} h(r,s,\gamma) R_{ii}(r,\delta)\, d\gamma \tag{3.12}$$

$$\Phi_{io}(r,s,\omega) = \frac{1}{2\pi}\int_{-\infty}^{\infty} h(r,s,\gamma)\, e^{-i\omega\gamma}\, d\gamma \int_{-\infty}^{\infty} R_{ii}(r,\delta)\, e^{-i\omega\delta}\, d\delta \tag{3.13}$$

$$\Phi_{io}(r,s,\omega) = \left[\int_{-\infty}^{\infty} h(r,s,\gamma)\, e^{-i\omega\gamma}\, d\gamma\right]\left[\frac{1}{2\pi}\int_{-\infty}^{\infty} R_{ii}(r,\delta)\, e^{-i\omega\delta}\, d\delta\right] \tag{3.14}$$

This yields

$$\Phi_{io}(r,s,\omega) = H(r,s,\omega)\,\Phi_{ii}(r,s,\omega) \qquad (3.15)$$

which indicates that the input-output cross-power density spectrum of a linear system is the product of the system function $H(r,s,\omega)$ and the input power density spectrum.

This is the relation used in computing the transfer function. The objective here is to indicate how this basic theorem may be extended to measure the response of mechanical systems under undeterministic loads that are functions of the space coordinates as well as of the time. This method also intends to give one an indication of the practicability of the computations involved and experimental procedures required to carry out the solution of the problem.

CHAPTER IV

EXPERIMENTAL INVESTIGATION

The physical models studied were a cantilever beam, shown in Figure 1, and a clamped square plate, shown in Figure 2. The support arrangements are depicted in these figures. The beam weighed 90 grams and measured 7 inches by 1 inch by 5/16 inch. It consisted of a lucite plastic inner core of 3/16 inch thickness cemented to an Armstrong vibration damping material 1/8 inch thick on either side of the plastic. The damping material, identified as #881-658 FF, decreased the time necessary to obtain acceptable correlation functions for spectral computation. A similar beam, without the damping material, called for time delays much larger than the afore-mentioned specimen. The 5-inch square plate weighed approximately 210 grams and was constructed of the same material as the beam. The total thickness was 1/4 inch.

The experimental flow chart is shown in Figure 3. The input data has been previously recorded on a loop spliced from a sample of the pressure signal sensed by a microphone 1/4 inch in diameter placed in a subsonic air jet [9]. This study presented statistical

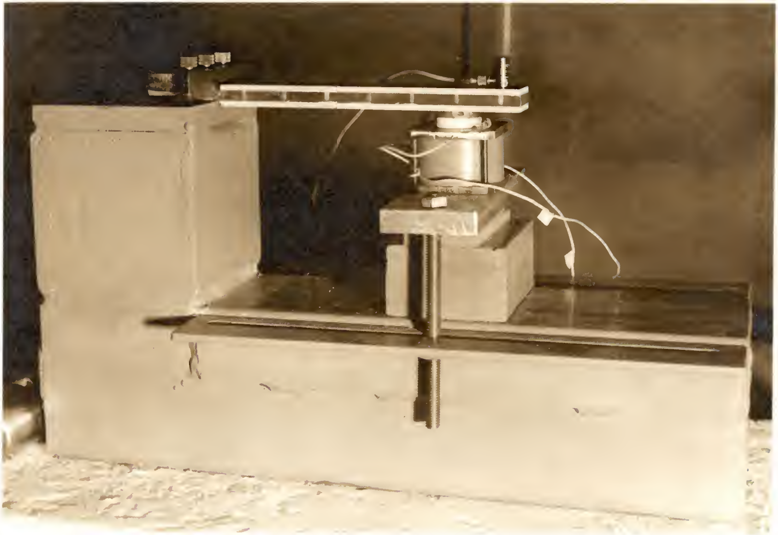

Figure 1. Beam Test Apparatus and Support

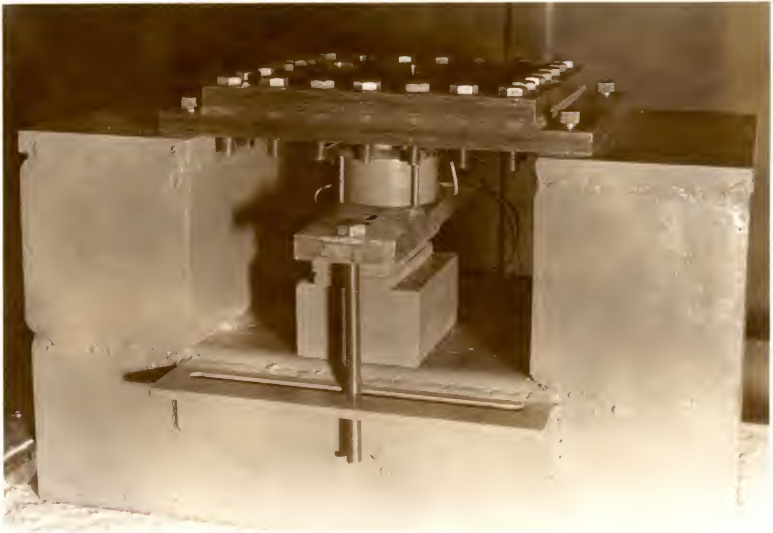

Figure 2. Plate Test Apparatus and Support

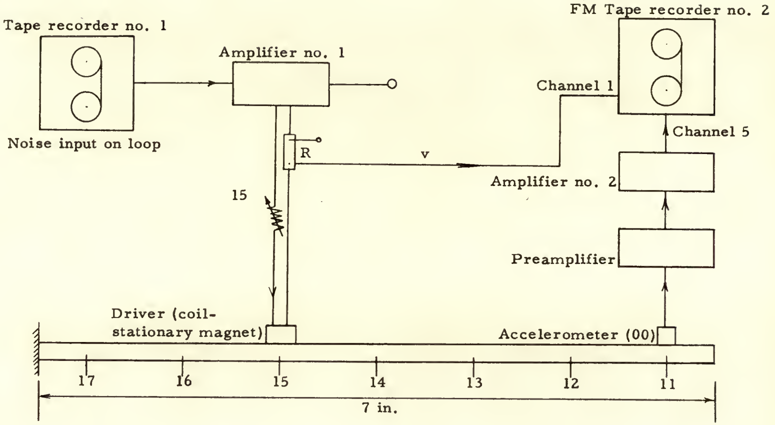

Figure 3. Experimental Flow Chart Showing Arrangement of Equipment

representations of pressures in an obstructed field [9]. It was this field that was taken to represent an actual service load on the structure. The transfer functions are computed by cross-correlation with this force under stationary conditions. The measurements of the pressure were made with two crystal microphones 1/4 inch in diameter, with a frequency range of 20 to 90,000 cycles per second. The two microphones provided simultaneous measurement of pressure, $p(r,t)$ at a pair of points, r and s, on the surface of a rigid plate. The data recording system is shown in Figure 4.

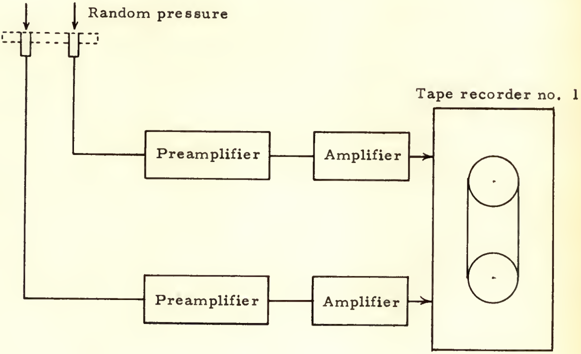

Figure 4. Recording of Random Pressure from a Subsonic Air Jet

A length of the magnetic tape was selected in which the process could be considered to be acceptably stationary, and then the tape was spliced into a loop which corresponded to 4 seconds in time at 60 inches/second. This time is called the recirculation time and is considerably greater than the averaging time (time constant) of the correlator. In Chapter VI the effect of analyzing a finite length loop is discussed in greater detail. The length of loop becomes important when considering the spectrum for low frequencies because the resonances of the structure on which the vibration is measured have extremely narrow bandwidths at this end of the spectrum.

Typical records of the signal and its autocorrelation are shown in Figures 5, 6 and 7. The signals were recorded simultaneously on a two-channel instrumentation tape recorder.

The transfer function was determined for one point--in the case of the beam, the free end, and for the plate, the center. A coordinate system was established so that position 0011 located the accelerometer. The signal was detected by a Massa accelerometer, model M-142B. This unit is designed so that it can be mounted on the beam through a tapped hole in the base of the unit. The response of the accelerometer is nearly unity because of the high frequencies of crystals. The sensitivity of the accelerometer coming out of the crystal is 2.88 mv/g. The additional mass of the accelerometer is

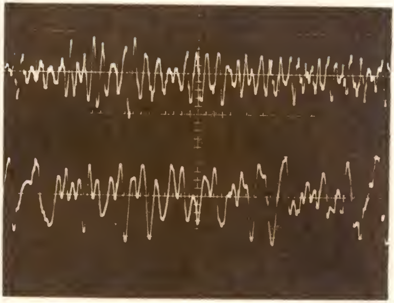

Figure 5. Oscilloscope Record of Force and Acceleration of Beam

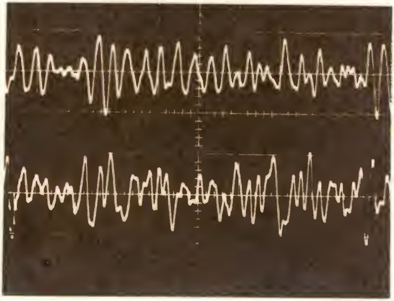

Figure 6. Oscilloscope Record of Force and Acceleration of Plate

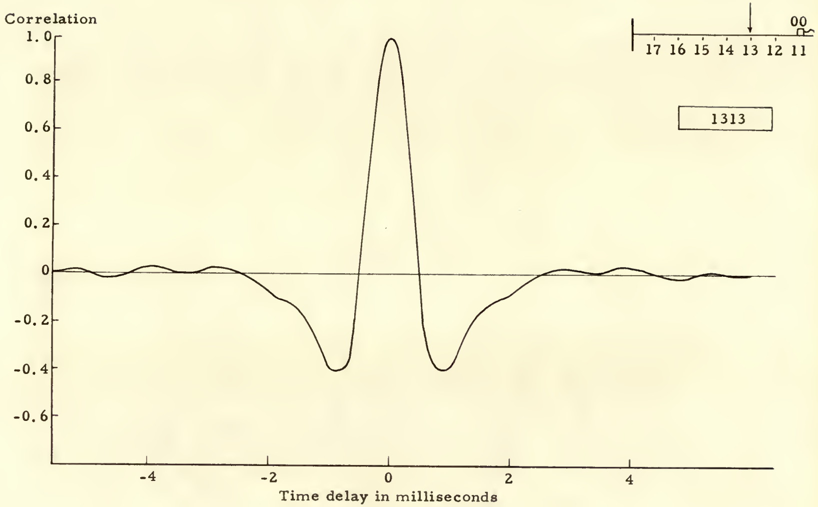

Figure 7. Autocorrelation of Force at Position 13

assumed to be negligible in comparison to that of the beam. It is reasonable to suspect that the accelerometer mass causes greatest error in the transfer function of the structure at the position 0011. This is the case when the force and accelerometer are at the free end.

The accelerometer is provided with an 18-inch low-noise microdot cable that is attached to the M-114B preamplifier. This preamplifier is designed with an extremely high frequency range so that it may be used in conjunction with the accelerometer and is properly protected and isolated from mechanical vibrations.

After amplification of the output of tape recorder no. 1, the signal was applied to an attached coil (4 grams) and stationary magnet driver unit as shown in Figure 3. The coil-magnet simulates the random force at the designated points. Since this arrangement acts as a shaker, it is heavily damped by the power amplifier and must be decoupled to prevent the coil-magnet from acting as a simple dashpot. This can be done by inserting an electrical resistance between the power amplifier and the coil as shown in Figure 3. The driver unit is moved after each simultaneous recording of the force and the acceleration.

In the study of the beam's dynamic characteristics the mass of the coil-magnet force-generator is neglected as was done for the case of the accelerometer mass. The ratio of the weight of the coil to the mass of the beam is small and justifies the above assumption. The determination of the autocorrelation of force at each point enables one to measure the disturbance of the force field caused by the movement of the beam. This is witnessed by the change in the spectral density of the force (see Figure 8). At first it was thought that one could compute the Fourier transformation of the autocorrelation at any one point and subsequently use this in the computation of $H(r,\omega)$. This cannot be done if one wishes to obtain accurate results.

The driver assembly permitted force-acceleration correlation at seven positions, spaced 1 inch apart along the beam. (The transfer functions at the free end, corresponding to these positions, are shown in Figures 24 through 37, Chapter VI.) For the plate, the same arrangement allowed cross-correlation at nine points, spaced approximately 1 inch apart over the plate. (The transfer functions at the center of the plate for these positions are shown in Figures 38 through 55, Chapter VI.)

Although the additional mass of shaker and accelerometer does not appreciably affect the dynamic characteristics of the beam, the same cannot be said of the plate. Because of the many resonances, plates have an extremely small driving-point impedance. Accurate measurements are difficult to obtain, particularly at the higher frequencies where the mass impedance of the coil exceeds the driving-

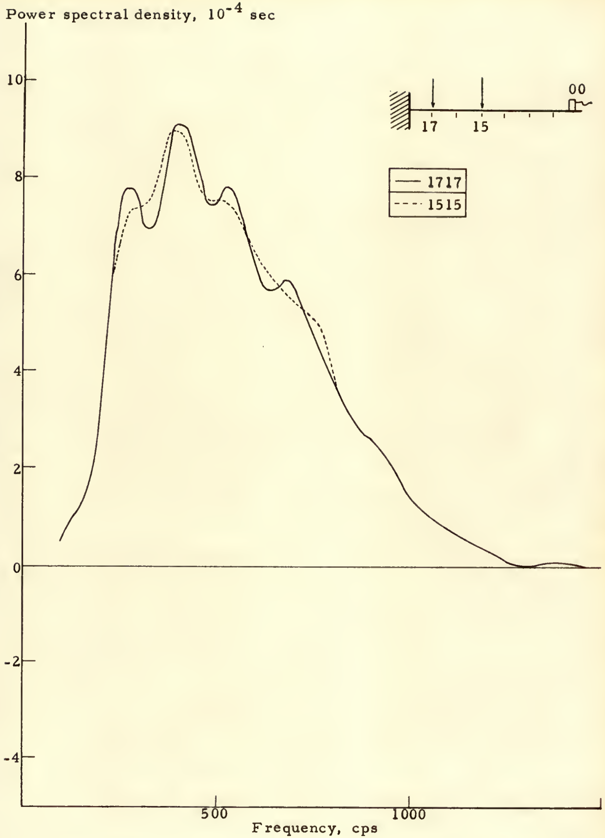

Figure 8. Structural Feedback Effect on Spectral Density Input

point impedance of the plate. As in the case of the beam, a resistance was placed in series with the coil-magnet arrangement in order to reduce the feedback from the coil to the amplifier as shown in Figure 3.

Correlation Measurement

The exact determination of the autocorrelation function or power spectral density would require an infinitely long sample. In addition, the sample must be assumed to be stationary. A single time function of the acceleration data was cut into loops of various smoothing times, T , and the correlation functions corresponding to these loops compared. For each loop the correlation was plotted and the Fourier transformation evaluated. Since this showed that there was no significant change in the spectral density, the samples could then be considered as approximately stationary for the short intervals of time. A signal whose averages, when performed on successive samples, show no change with time is called a stationary signal. Thus the correlation can be written as

$$R_{io}(r,\tau) = \overline{f_i(r,t)\cdot f_o(r,t+\tau)} = \lim_{T\to\infty} \frac{1}{2T}\int_{-T}^{+T} f_i(r,t) f_o(r,t+\tau)\,dt \qquad (4.1)$$

Since the smoothing time is fixed, the correlation curves are no more than estimates of the true correlation. The normalized value of $R(r,\tau)$ is obtained by dividing the time average of the two signals, $f_i(r,t)$

and $f_o(r,t)$, by the rms value of each of these signals. The normalized correlation takes the following form for electronic computation:

$$R_{io}(r,\tau) = \frac{\overline{f_i(r,t-\tau)\,f_o(r,t)}}{\left\{\overline{\left[f_i(r,t)\right]^2}\;\overline{\left[f_o(r,t)\right]^2}\right\}^{1/2}} \tag{4.2}$$

The length of record, T, was chosen as 4 seconds. The lag, τ, was taken at values less than 0.5 per cent of the length of the sample. Theoretically, the computation of $R_{io}(r,\tau)$ is valid only for $|\tau| \leq T_m < T$, where T_m is the maximum desirable lag. The block diagram for this operation is displayed in Figure 9.

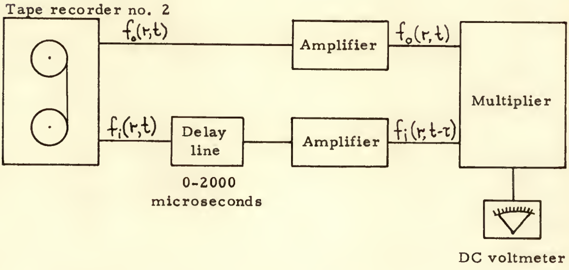

Figure 9. Flow Diagram for the Evaluation of Correlation

The acceleration, $f_i(r,t)$, and force, $f_o(r,t)$, are played back simultaneously from channels 1 and 5, respectively, of the Ampex FR-1100 Recorder/Reproducer system. The recorder is equipped with seven channels. The appropriate time shift was introduced by an audio delay line with a time delay range of 0 to 2000 microseconds on either of the two signals. The two signals were multiplied with a Philbrick Multiplying/Dividing component with a 15 kc bandpass. The time average of the multiplier output is formed by a dc vacuum-tube voltmeter. The rms values of the respective signals were found by the same procedure as above, except that the time shift, τ, was not introduced.

It may be observed from Figure 10 that the time delay, τ, is extended to 10 milliseconds. This large delay is made possible by delaying a signal for 2000 microseconds and then recording it on another channel. This can be repeated as often as desired, since the fm track will erase any previous signal as it records. Thus, a 2000-microsecond delay in the force is recorded on channel 5, and at the same time the acceleration is recorded on channel 7 without delay. In the computation of the correlation function, the interchannel time displacement error must be taken into account. This is caused by the misalignment of the track heads. Misalignment produced a time delay error as large as 25 microseconds.

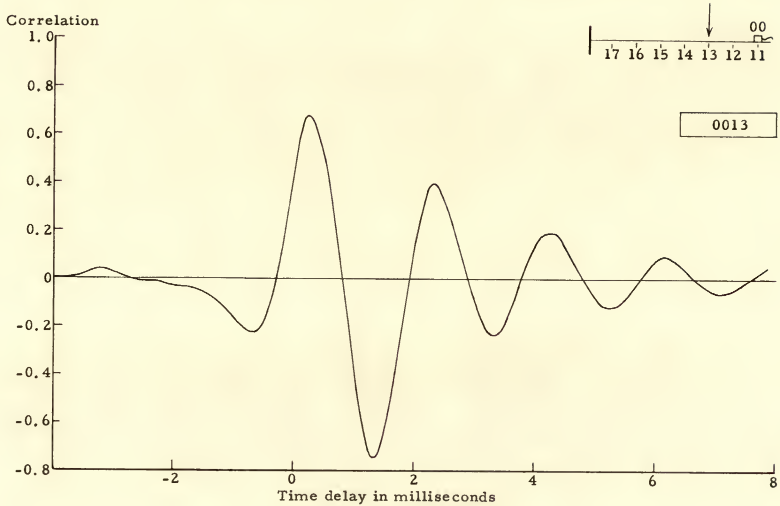

Figure 10. Cross-Correlation of Force-Acceleration

A comparison of correlation functions plotted for different smoothing times showed that the quality of the spectral density estimate does not increase insofar as the computation of the transfer function is concerned.

The acceleration and force were recorded for 20 seconds at a tape speed of 30 ips. These records were cut and spliced into 4-second loops. During the playback process, the tape speed was increased to 60 ips.

Power Spectral Measurement

It was previously mentioned that a theoretically accurate determination of the power spectral density requires an analysis of a stationary random phenomenon during an infinite time interval. Since this cannot be done, the results obtained are estimates of the power spectrum, even though the operations involved in the process are exact.

After the correlation function was obtained, the Fourier transformation required for establishment of the power spectral density was performed on the IBM 650 computer. The computation is incorporated in the following formula:

$$\Phi_{mn}(f) = \int_0^\infty \left[R_{mn}(\tau) + R_{nm}(\tau) \right] \cos 2\pi f \tau \, d\tau + i \int_0^\infty \left[R_{nm}(\tau) - R_{mn}(\tau) \right] \sin 2\pi f \tau \, d\tau \qquad (4.3)$$

The integral is divided into a finite series over an interval, $\Delta\tau$, where

$$\tau_k = k\,\Delta\tau \qquad k = 0, 1, 2, \ldots$$

The final numerical computation for the cross-power spectral density becomes

$$\Phi_{xy}(\omega) = \Delta\tau\left[R_{xy}(0) + \sum_{k=1}^{n}\left(R_{xy}^{k} + R_{yx}^{k}\right)\cos\omega\tau_k\right] + i\,\Delta\tau\sum_{k=1}^{n}\left(R_{yx}^{k} - R_{xy}^{k}\right)\sin\omega\tau_k \tag{4.4}$$

where $\Delta\tau$ is taken as 40×10^{-6} seconds. When $x = y$, Φ_{xx} becomes the power spectral density,

$$\Phi_{xx}(\omega) = 2\Delta\tau\left[\tfrac{1}{2} + \sum R_{xx}^{k}\cos\omega\tau_k\right] \tag{4.5}$$

A typical set of curves computed from the above formulas for several positions on the beam is shown in Figures 11 through 15. Similar curves are indicated in Figures 16, 17 and 18 for the plate.

It should be mentioned that the cross-power spectrum cannot be interpreted as a transfer of power between different parts of the

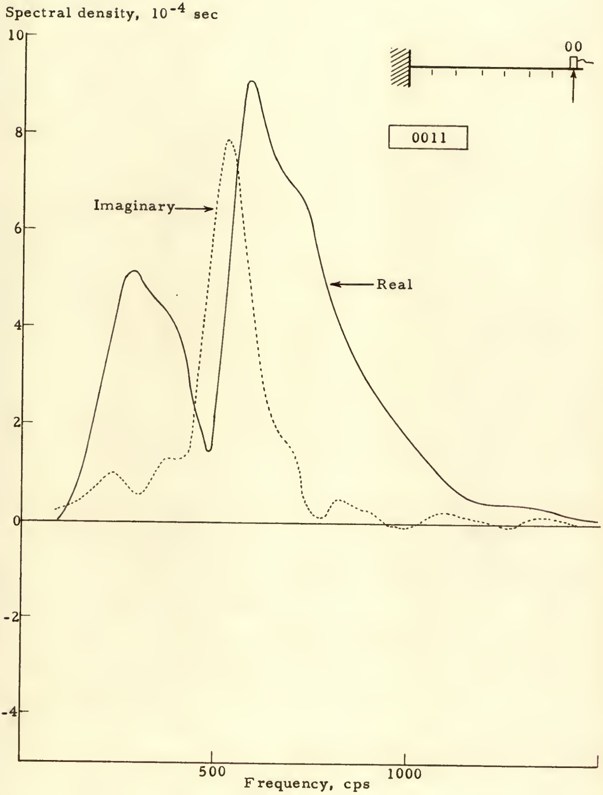

Figure 11. Cross-Power Spectral Density of Force-Acceleration

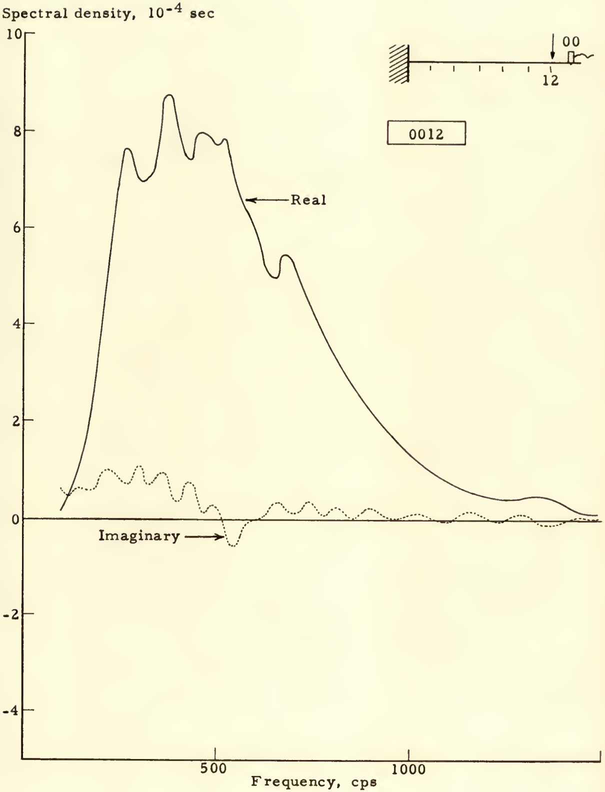

Figure 12. Cross-Power Spectral Density of Force-Acceleration

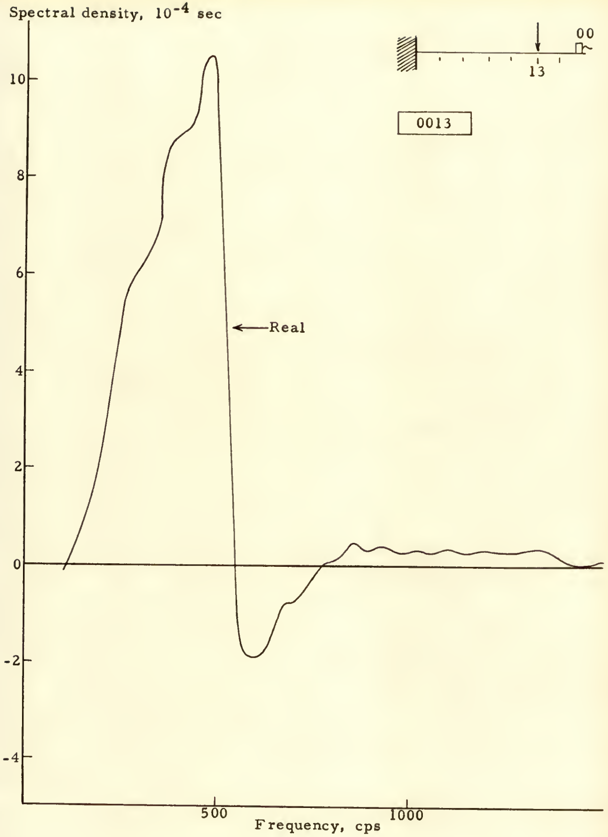

Figure 13. Cross-Power Spectral Density of Force-Acceleration

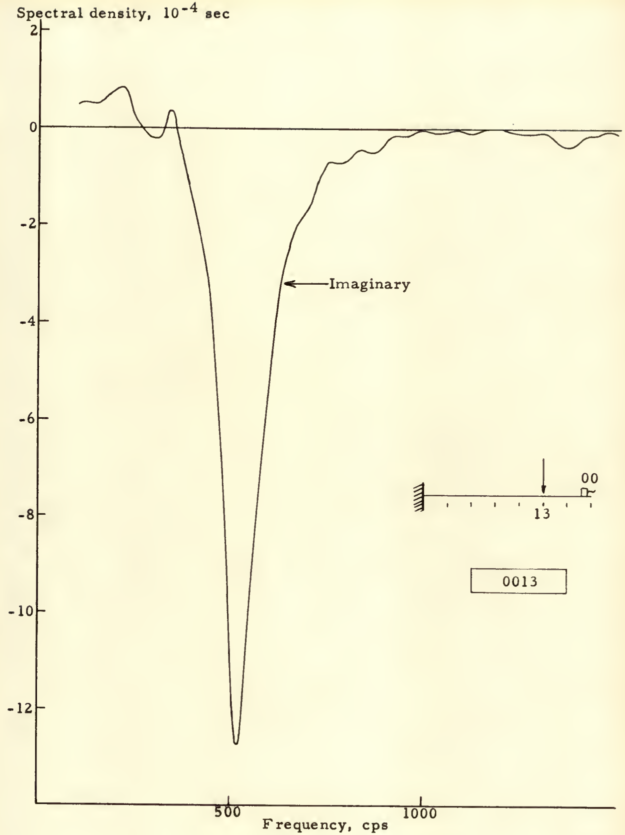

Figure 14. Cross-Power Spectral Density of Force-Acceleration

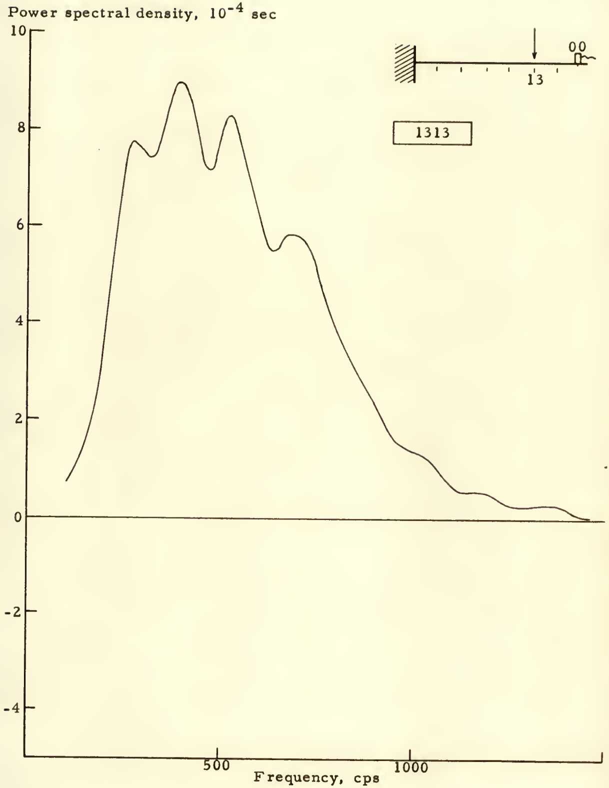

Figure 15. Power Spectral Density of Input Force

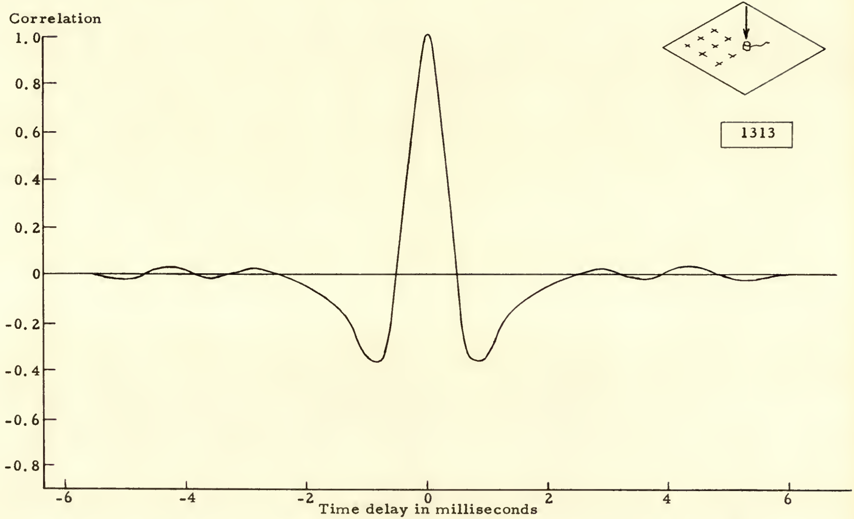

Figure 16. Autocorrelation of Force

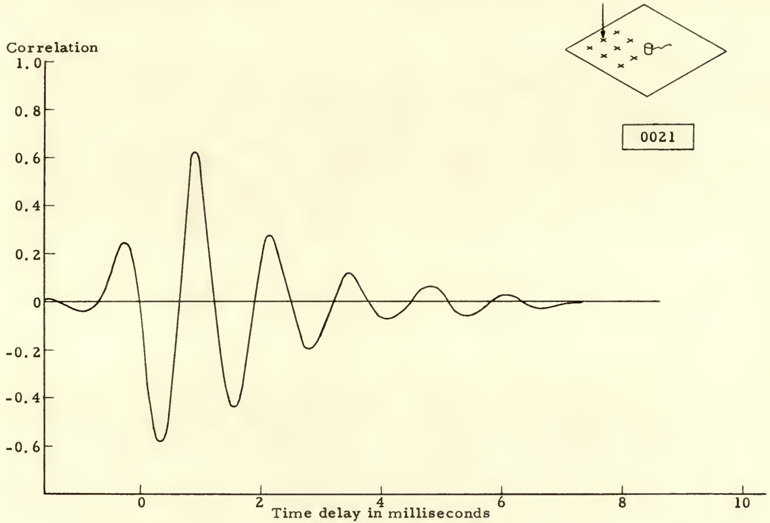

Figure 17. Cross-Correlation of Force-Acceleration

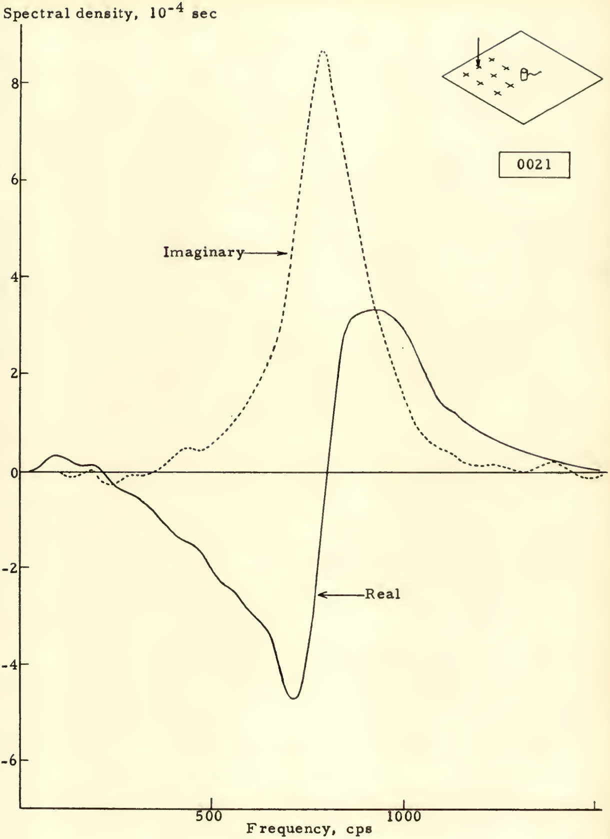

Figure 18. Cross-Power Spectral Density of Force-Acceleration

structure or the spectrum of power taken by the structure. Although the cross-correlation, R_{xy} , after transformation, has the same dimensions as power, it does not yield a spectrum of power. The input force and output acceleration are cross-correlated at different locations on the structure merely for transfer function determinations.

CHAPTER V

NORMAL MODE DETERMINATION OF THE TRANSFER FUNCTION

An attempt has been made to compare the beam transfer function as determined from the cross-correlation theorem with a model that is established in terms of a simple harmonic motion.

Referring to the analysis on page 12, equation (2.22), the response $\Phi_o(r,s,\omega)$ can be written as

$$\Phi_o(r,s,\omega) = \iint \sum_{i,j,l,m} \frac{V_{ij}(r)\,V_{ij}(r_2)\,V_{lm}(s)\,V_{lm}(s_2)}{b_{ij}\,b_{lm}\left(\lambda_{ij}^2-\omega^2-2i\beta\omega\right)} \tag{5.1}$$

$$\frac{\Phi_i(r,s,\omega)\,dr_2\,ds_2}{\left(\lambda_{lm}^2-\omega^2+2i\beta\omega\right)}$$

This can be rewritten as

$$\Phi_o(r,s,\omega) = \iint \left[\sum_{i,j} \frac{V_{ij}(r)\,V_{ij}(r_2)}{b_{ij}\left(\lambda_{ij}^2-\omega^2-2i\beta\omega\right)}\right] \tag{5.2}$$

$$\left[\sum_{l,m} \frac{V_{lm}(s)\,V_{lm}(s_2)}{b_{lm}\left(\lambda_{lm}^2-\omega^2+2i\beta\omega\right)}\right]\Phi_i(r_2,s_2,\omega)\,dr_2\,ds_2$$

Equation (5.2) is put in the following form, where the conjugate is denoted by an asterisk (*):

$$\Phi_o(r_1,s_1,\omega) = \iint H(r_1,r_2,\omega)\,H^*(s_1,s_2,\omega)\,\Phi_i(r_2,s_2,\omega)\,dr_2\,ds_2 \qquad (5.3)$$

The complex frequency response is

$$H(r,\omega,m) = \sum_m \frac{V_m(x)\,V_m(\eta)}{4\pi^2 l}\left\{\frac{1-(f/f_m)^2-2iD(f/f_m)}{\left[1-(f/f_m)^2\right]^2+4D^2(f/f_m)^2}\right\} \qquad (5.4)$$

where D is a dimensionless damping factor.

In this form the transfer function $H(r,\omega,m)$ is readily seen to be a superposition of modes, each considered to be a single degree-of-freedom system with a particular natural frequency and damping characteristic as shown in Figures 19 and 20. Equation (5.4) expresses the transfer function for displacement of the beam. To find the transfer function for acceleration, we can make use of the following expressions for derivatives of correlation functions. Starting with the definition of the cross-correlation,

$$R_{io}(\tau) = \lim_{T\to\infty}\frac{1}{2T}\int f_i(r,t)\,f_o(r,t+\tau)\,dt \qquad (5.5)$$

and differentiating under the integral sign, we have

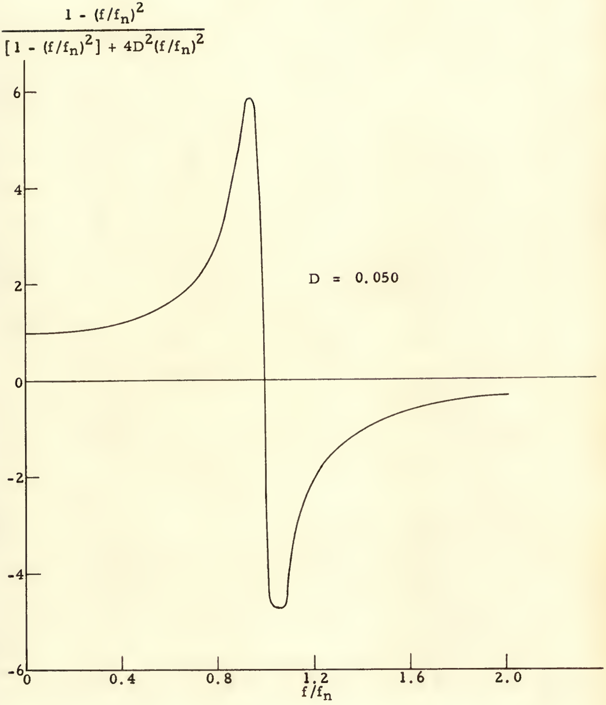

Figure 19. Real Part of Beam Response Represented as a Single Degree-of-Freedom System

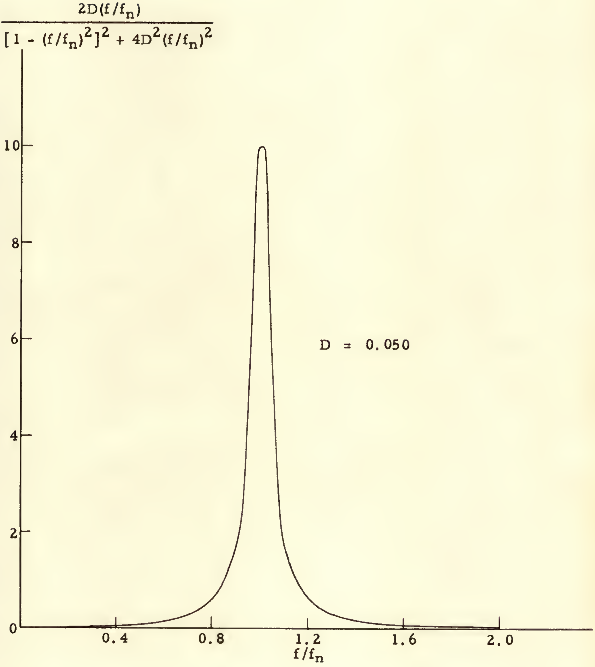

Figure 20. Imaginary Part of Beam Response Represented as a Single Degree-of-Freedom System

$$\frac{d}{d\tau}\left[R_{io}(\tau)\right] = \lim_{T\to\infty}\frac{1}{2T}\int_{-T}^{+T} f_i(r,t)\,f_o'(r,t+\tau)\,dt \tag{5.6}$$

where $d/d\tau\left[R_{io}(\tau)\right] = R_{io}'(\tau)$ and $d/d\tau(f_o) = f_o'$. A second differentiation under the integral sign gives

$$\frac{d^2}{d\tau^2}\left[R_{io}(\tau)\right] = R_{io}''(\tau) = \lim_{T\to\infty}\frac{1}{2T}\int_{-T}^{T} f_i(r,t)\,f_o''(r,t+\tau)\,dt \tag{5.7}$$

Thus the second derivative of the cross-correlation of the force and displacement is another cross-correlation between force and acceleration.

To find the corresponding relation in the frequency domain, we write

$$R_{io}(\tau) = \int_{-\infty}^{\infty} \Phi_{io}(\omega)\,e^{+j\omega\tau}\,d\omega \tag{5.8}$$

and differentiate both sides twice; thus,

$$R_{io}''(\tau) = \int_{-\infty}^{\infty} (j\omega)^2\,\Phi_{io}(\omega)\,e^{+j\omega\tau}\,d\omega \tag{5.9}$$

Taking the inverse transform, we obtain

$$2\pi(j\omega)^2 \Phi_{io}(\omega) = \int_{-\infty}^{\infty} R''_{io}(\tau)\, e^{-j\omega\tau}\, d\tau \tag{5.10}$$

Since

$$\Big[H(r,\omega)\Big]_{displ.} = \frac{\Phi_{io}(r,\omega)}{\Phi_{ii}(r,\omega)} \tag{5.11}$$

the corresponding $H(r,\omega)$ for acceleration is given by

$$\Big[H(r,\omega)\Big]_{acc.} = -\omega^2 \Big[H(r,\omega)\Big] \tag{5.12}$$

The theoretical and experimental transfer functions are plotted for the acceleration response (see Figures 24 through 56, Chapter VI).

TABLE 1

EXPERIMENTALLY DETERMINED BEAM PARAMETERS

Mode n	Measured Frequency	Ratio to First Mode Frequency	Damping Factor (D)	β_n
1	24.2	1.0	0.0442	6.64
2	158.0	6.5	0.0446	44.10
3	430.0	17.9	0.0450	109.50
4	910.0	37.9	0.0500	285.00
5	1450.0	60.4	0.0519	473.00
6	2250.0	93.9	0.0555	734.00

Table 1 lists the natural frequencies found experimentally. A Tektronix dual-beam oscilloscope was used in conjunction with a wide-range oscillator to produce the Lissajous' figures between the input and output acceleration. In Table 1 the first six modes are listed.

To determine the damping of each mode, use was made of a Dumont oscillograph record camera. The beam is excited at its natural frequency with a steady-state sinusoidal input. At a predetermined time, a circuit was opened which triggered the sweep on the oscilloscope, and this permitted a record of the transient vibration to be obtained. Figures 21 and 22 show a record of a transient at a frequency of 62 and 940 cycles per second, respectively. To determine the damping coefficient for a particular mode, it is assumed that the beam acts as a single degree-of-freedom system. This is approximately true for a natural vibration. Thus, the differential equation that follows defines the model:

$$\ddot{q} + 2DK\dot{q} + K^2 q = 0 \tag{5.13}$$

where

q = lateral displacement

K = natural frequency

D = damping factor.

$$\lambda_{1,2} = -DK \pm \sqrt{D^2K^2 - K^2}$$

$$\lambda_{1,2} = -K\left(D \mp i\sqrt{1-D^2}\right)$$

$$\lambda_{1,2} = -\beta_n \pm i\nu$$

$$\therefore \quad \beta_n = KD$$

$$\nu = K\sqrt{1-D^2}$$

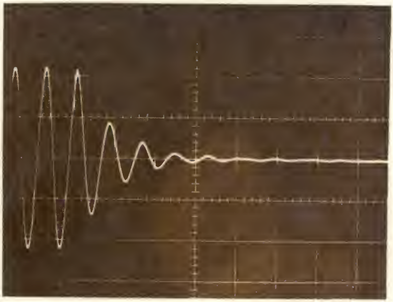

Figure 21. Oscilloscope Record of Beam Transient for Second Mode

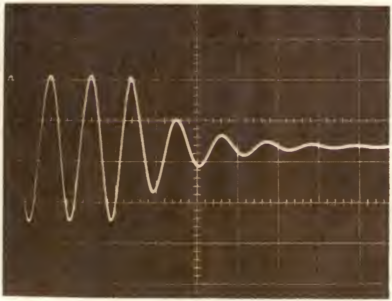

Figure 22. Oscilloscope Record of Beam Transient for Third Mode

The solution of this equation is written as

$$q = C e^{-\beta_n t} \cos(\nu t + \alpha) \tag{5.14}$$

If we denote by $q_1, q_2, q_3, \ldots, q_k$ the successive maximum displacements on the same side of the axis, the ratio of the $q_k^{th.}$ amplitude to the $q_{k+1}^{th.}$ amplitude will be given as

$$\frac{q_k}{q_{k+1}} = \frac{q_k}{q_k e^{-\beta_n T'}} = e^{+\beta_n T'} \tag{5.15}$$

where

$$T' = T/\sqrt{1-D^2} = 2\pi/K\sqrt{1-D^2} = 2\pi/\nu$$

and

$$T = 2\pi/K$$

Here $\nu = K\sqrt{1-D^2}$ represents the circular frequency in the presence of damping.

The logarithmic decrement I is found from

$$I = \ln \frac{q_k}{q_{k+1}} = \left(\frac{2\pi}{\sqrt{1-D^2}\,K}\right)\beta_n = \frac{2\pi D}{\sqrt{1-D^2}} \tag{5.16}$$

Figure 23 indicates the determination of D for the second mode at a frequency of 158 cycles per second. Values of successive amplitudes are read directly from the oscillograph records, Figures 21 and 22.

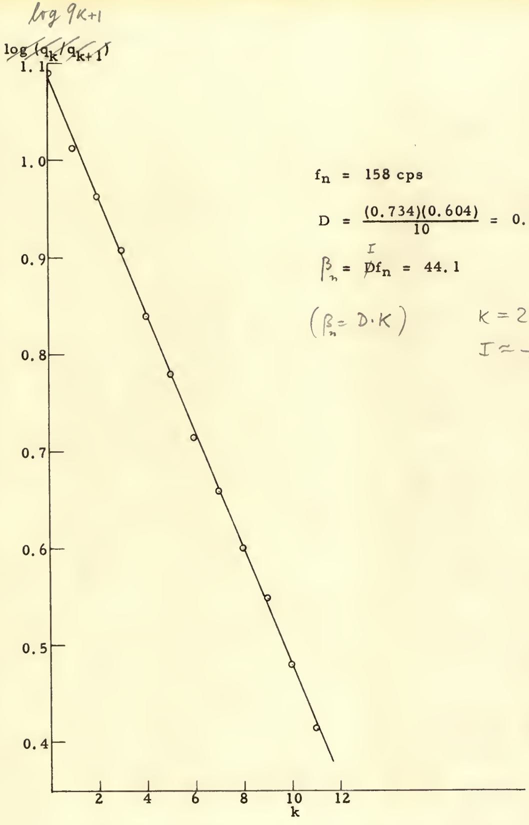

$f_n = 158$ cps

$D = \frac{(0.734)(0.604)}{10} = 0.0446$?

$\beta_n = \overset{I}{\cancel{D}} f_n = 44.1$

$(\beta_n = D \cdot K)$

$K = 2\pi f_n$

$I \approx \frac{D}{2\pi}$

Figure 23. Plot of Logarithmic Decrement for the Second Mode of Vibration

The slope of the curve gives the damping coefficient ~~β~~ D *). The value of ~~D~~ β is determined by multiplying ~~β~~ D by the natural frequency in radians per second. The following calculation of $H(r,\omega,m)$ does not assume that the damping coefficient is constant for all modes, as is usually the case. Table 1 lists the damping coefficients for each respective mode.

The characteristic functions representing the normal modes of a cantilever beam have been computed by Young and Felgar [10]. Tables 2, 3, 4, 5 and 6 show a sample computation of $H(r,\omega)$ at frequencies of 500, 1000 and 1500 cycles per second. In Chapter VI the results of the modal solution are represented by the dotted curve.

*) according to

$$I = \frac{2\pi D}{\sqrt{1-D^2}} \approx 2\pi D \text{ for small } D$$

$$\beta_n = KD \approx \cancel{2\pi} f_n \frac{I}{\cancel{2\pi}} = I f_n$$

TABLE 2

REAL (R) AND IMAGINARY (I) PARTS OF THE TRANSFER FUNCTION

f/f_n	0.1	0.3	0.5	0.6	0.7	0.8	1.0
$2D\,f/f_n$	0.01	0.03	0.05	0.06	0.07	0.08	0.1
$(f/f_n)^2$	0.01	0.09	0.25	0.36	0.49	0.64	1.0
$1-(f/f_n)^2$	0.99	0.91	0.75	0.64	0.51	0.36	0
$[1-(f/f_n)^2]^2$	0.9801	0.8281	0.5625	0.4096	0.2601	0.1296	0
$\alpha^2 = 4D^2(f/f_n)^2$	0.0001	0.0009	0.0025	0.0036	0.0049	0.0064	0.010
$1-(f/f_n)^2+\alpha^2$	0.9802	0.8290	0.5650	0.4132	0.2650	0.1360	0.010
R	1.0099	1.0977	1.3274	1.5489	1.9245	2.6471	0
I	0.0102	0.03618	0.08849	0.14520	0.26415	0.5882	10

$$R_n = \frac{(1 - f^2/f_n^2)}{[1-(f/f_n)^2]^2 + 4D^2(f/f_n)^2} \qquad I_n = \frac{2D\,f/f_n}{[1-(f/f_n)^2]^2 + 4D^2(f/f_n)^2}$$

TABLE 3

CHARACTERISTIC MODE SHAPES FOR CANTILEVER BEAM

Position	0017	0016	0015	0014	0013	0012	0011
x/ℓ	0.0715	0.214	0.357	0.50	0.643	0.786	0.928
V_1	0.017	0.145	0.375	0.679	1.032	1.413	1.814
V_2	0.101	0.668	1.256	1.427	0.9774	-0.019	-1.312
V_3	0.259	1.289	1.340	0.039	-1.204	-0.912	+0.878
V_4	0.460	1.502	0.068	-1.414	-0.017	1.311	-0.447
V_5	0.680	1.149	-1.261	0.002	1.272	-1.051	+0.034

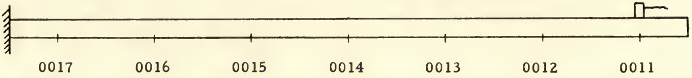

TABLE 4

COEFFICIENTS OF $a_n = \frac{V_n(x/\ell)\ V_n(x/\ell)}{f_n^2}$

Mode	$2 f_n$	$\frac{V(\eta/\ell)}{f_n^2} \times 10^6$	$V(x/\ell)$ 0011	$a_n \times 10^6$ 0011	$V(x/\ell)$ 0012	$a_n \times 10^6$ 0012
1	48	+785.7	+1.814	+1425.26	+1.413	+1110.194
2	316	-13.138	-1.312	+17.237	-0.019	+0.2496
3	860	+1.187	+0.878	+1.0422	-0.912	-1.0825
4	1820	-0.1349	-0.447	+0.0603	+1.311	-0.1769
5	2900	+0.00403	+0.034	+0.00014	-1.051	+0.0042

TABLE 4--Continued

Mode	$2f_n$	$\frac{V(n/\ell)}{f_n^2} \times 10^6$	$V(x/\ell)$ 0013	$a_n \times 10^6$ 0013	$V(x/\ell)$ 0014	$a_n \times 10^6$ 0014
1	48	+785.7	+1.032	+810.842	+0.679	+533.490
2	316	-13.138	+0.9774	-12.841	+1.427	-18.748
3	860	+1.187	-1.204	-1.429	+0.039	+0.0463
4	1820	-0.1349	-0.017	+0.00229	-1.414	+0.19075
5	2900	+0.00403	+1.272	+0.00512	+0.002	+0.00001

TABLE 4--Continued

Mode	f_n	$\frac{V(n/\ell)}{f_n^2} \times 10^6$	$V(x/\ell)$ 0015	$a_n \times 10^6$ 0015	$V(x/\ell)$ 0016	$a_n \times 10^6$ 0016
1	48	+785.7	+0.375	+294.6375	+0.145	+113.9265
2	316	-13.138	+1.256	-16.501	+0.668	-8.776
3	860	+1.187	+1.340	+1.5906	+1.289	+1.530
4	1820	-0.1349	+0.068	-0.00817	+1.502	-0.20262
5	2900	+0.00403	-1.261	-0.00508	+1.149	+0.00463

TABLE 4--Continued

Mode	f_η	$\frac{V(\eta/\ell)}{f_\eta^2} \times 10^{-6}$	$V(x/\ell)$ 0017	$a_\eta \times 10^{-6}$ 0017
1	48	+785.7	+0.017	+13.357
2	316	-13.138	+0.101	-1.3269
3	860	+1.187	+0.259	+0.3074
4	1820	-0.1349	+0.460	-0.0621
5	2900	+0.00403	+0.680	+0.00274

TABLE 5

CONTRIBUTION OF THE N^{th} MODE TO THE TRANSFER FUNCTION

Mode	f/f_n	R_n	I_n
$f = 500$			
1	10.416	-0.00930	+0.000078
2	1.5822	-0.6594	+0.0624
3	0.5814	+1.5010	+0.1187
4	0.2747	+1.0807	+0.0321
5	0.1724	+1.0303	+0.0190
$f = 1000$			
1	20.833	-0.00231	0
2	3.1646	-0.1109	+0.00350
3	1.1628	-2.6095	+0.7755
4	0.5494	+1.4235	+0.11202
5	0.3448	+1.1331	+0.04611
$f = 1500$			
1	31.25	-0.0010	0
2	4.7468	-0.0464	+0.00092
3	1.7442	-0.48678	+0.037417
4	0.8242	+2.9250	+0.75170
5	0.5172	+1.3578	+0.09970

TABLE 6

REAL AND IMAGINARY COMPONENTS OF THE TRANSFER FUNCTION FOR ACCELERATION AND DISPLACEMENT CONSIDERING PARTICIPATION OF FIVE MODES OF VIBRATION

Position	$Hx10^{-6}$	f = 500	f = 1000	f = 1500
0011 Displacement	Real Imaginary	-22.555 +1.315	-7.753 +0.875	-2.5526 +0.100
0011 Acceleration	Real Imaginary	+5.6388 -0.3288	+7.753 -0.875	+5.743 -0.225
0012 Displacement	Real Imaginary	-12.220 -0.030	+0.041 -0.858	-1.102 -0.173
0012 Acceleration	Real Imaginary	+3.055 +0.0075	-0.041 +0.858	+2.480 +0.389
0013 Displacement	Real Imaginary	-1.157 -0.906	+3.265 -1.153	+0.494 -0.063
0013 Acceleration	Real Imaginary	+0.2893 +0.2265	-3.265 +1.153	-1.112 +0.142
0017 Displacement	Real Imaginary	+1.148 -0.047	-0.771 +0.227	-0.279 -0.236
0017 Acceleration	Real Imaginary	-0.2870 +0.0118	+0.771 -0.227	+0.628 +0.081

CHAPTER VI

PRESENTATION AND DISCUSSION OF EXPERIMENTAL RESULTS

It is evident from this study that precise data reduction of a random vibration with an irregularly shaped spectrum of force is a slow process, although it can be made automatic. The time needed to produce a correlation curve is approximately 2 hours. The raw vibration data are obtained on magnetic tape, and in preparing for a harmonic analysis a brief portion of the tape is spliced into a loop. The loop, when played back, has a definite recirculation frequency f_r, even though the actual measurement is assumed random. In order to estimate the error imposed by the finite integration time, we may assume that the correlation curves shown in Figures 10 and 17 are exponential-cosine functions and are obtained from a normal random process. It can be shown that the mean square variation, σ_{xy}^2 , about the mean value of a set of measurements is given by the following formula [1]:

$$\sigma_{xy}^2(\tau,T) = \langle {}^k R_{xy}^2(\tau,T) \rangle - R_{xy}^2(\tau) \qquad (6.1)$$

where k denotes the different ensemble members.

With the assumption of an exponential correlation, this reduces to

$$\sigma_{xx}^2(\alpha,\beta) = \frac{2\beta - 1 + 2e^{-2\beta} + \left[(2\alpha+1)(2\beta-1) - 2\alpha^2\right]}{2\beta^2} \qquad (6.2)$$

where the dimensionless parameters α and β are

$$\alpha = \pi B \tau$$
$$\beta = \pi B T$$

This is an exact expression for all α and β for which the delay τ is less than the smoothing time T. For the loop under consideration, the smoothing time is approximately 4 seconds, and the bandwidth of the correlator is about 15,000 cycles per second, considered as the bandpass of the multiplier. Thus,

$$\beta \doteq \pi B T \doteq \pi(15{,}000)(4) \doteq 2 \times 10^5 \qquad (6.3)$$

This value of β is sufficiently large [1, p. 269] to justify use of the formula developed by Bendat [1, p. 268], i.e.,

$$\sigma_{xx}^2(\alpha,\beta) = \frac{k}{\beta} \qquad 1<k<2 \qquad (6.4)$$

The expected rms error in a set of measurements of the autocorrelation function at any point along the autocorrelation curve for $k=2$ is $\sigma_{xx}(\alpha,\beta) = 0.0045$ [1, Table 7.2, p. 269].

For all values of T and τ, the output signal-to-noise amplitude ratio of the correlator is defined as the ratio of the expected mean value to the standard deviation, that is,

$$\left(\frac{R}{\sigma}\right)_{out.} = \frac{R_{xy}(\tau)}{\sigma_{xy}(\tau, T)} \tag{6.5}$$

For an exponential correlation curve, this becomes

$$\left(\frac{R}{\sigma}\right)_{out.} = \frac{e^{-\alpha}}{\sigma_{xx}(\alpha,\beta)} \tag{6.6}$$

Since $\beta = 2 \times 10^5$ and is thus considered large, we can substitute (6.4) into (6.6) for $\sigma_x(\alpha,\beta)$. Thus

$$\left(\frac{R}{\sigma}\right)_{out.} = e^{-\alpha}\left(\frac{\beta^{1/2}}{k^{1/2}}\right) \tag{6.7}$$

for large β.

This formula gives a signal-to-noise ratio of 1.5 for $\alpha = 5$. It shows that the accuracy in the correlation measurement drops off quickly for values α greater than 5. This result indicates that the output signal-to-noise ratio will be less than 1.5 for a time delay greater than 100 microseconds. The exponential correlation function represents an upper bound in evaluating the statistical error measurement of the correlation function. It is reasonably safe to say that the errors for an exponential-cosine correlation will be much less than those obtained above and will not give erroneous results for $H(r,\omega)$

In determining the autocorrelation at different locations along the structure, it was found that the system disturbs the force field. This was shown in Figure 8 by the comparison of two spectral density curves of input force. The autocorrelation must be evaluated at every point in order to account for the disturbance created by the structure.

The resulting transfer functions for a cantilever beam and clamped plate are shown in Figures 24 through 56. The graphs show the amplitude and phase as a function of frequency in cycles per second. Each graph indicates the spacewise contribution to the transfer function. In Figures 24 through 30 the dotted curves represent the analysis of Chapter V for the modal vibration. At position 0017 the theoretical solution deviates considerably from the experimental curve. The normal modes, $V_m(x/\ell)$, introduced into the solution are for a fixed-free beam. Because the experimental beam is, of course, not completely fixed, it is to be expected that the V_m in the proximity of the support do not give an accurate description of the experimental characteristic shapes. For points far from the fixed end the results agree favorably with an assumed fixed-free beam. The partially clamped end has little effect near the latter region.

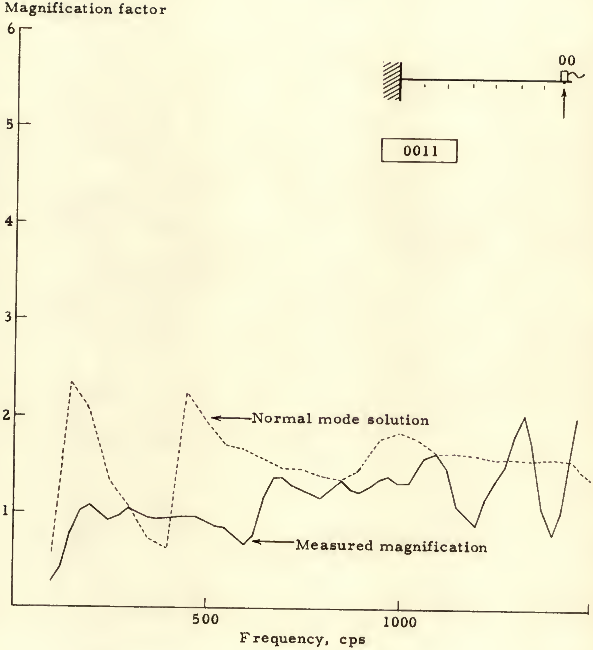

Figure 24. Modulus of Acceleration Transfer Function at 0011

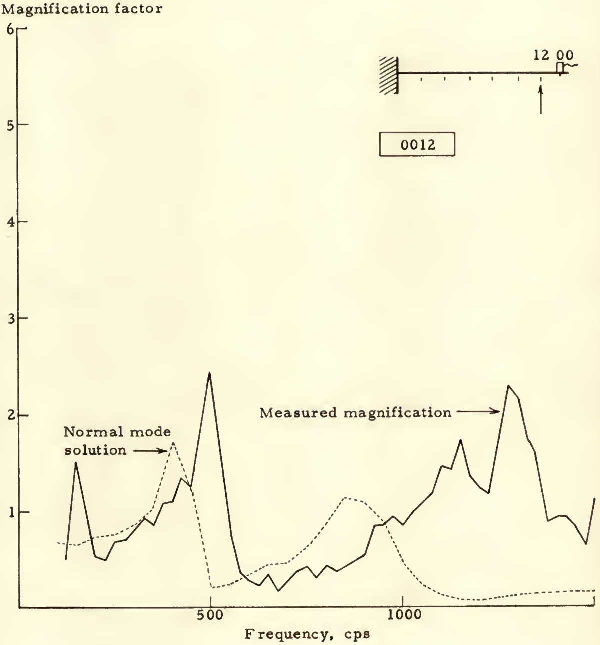

Figure 25. Modulus of Acceleration Transfer Function at 0012

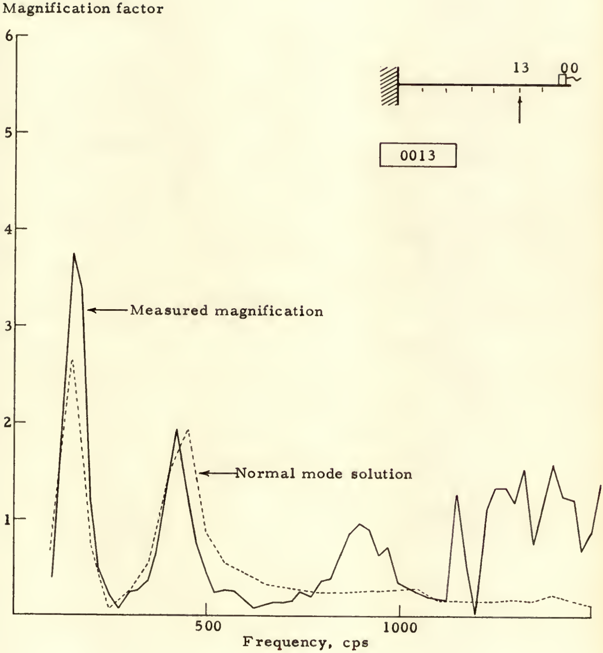

Figure 26. Modulus of Acceleration Transfer Function at 0013

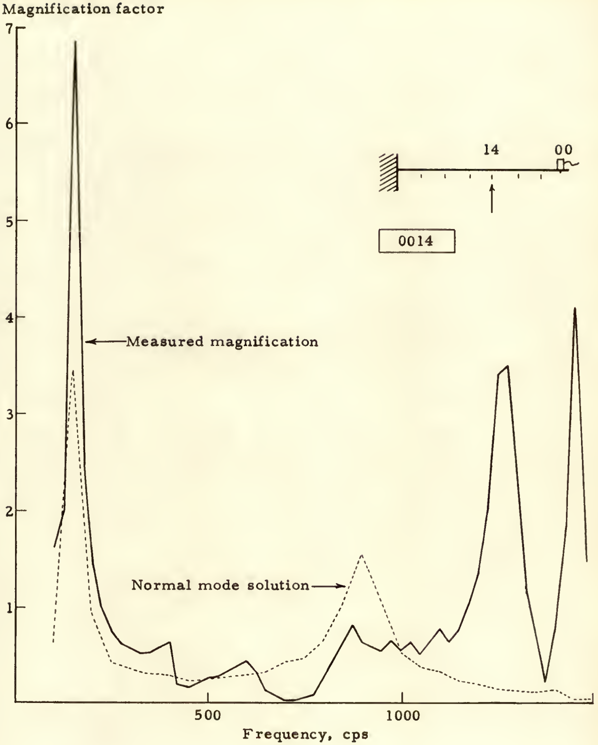

Figure 27. Modulus of Acceleration Transfer Function at 0014

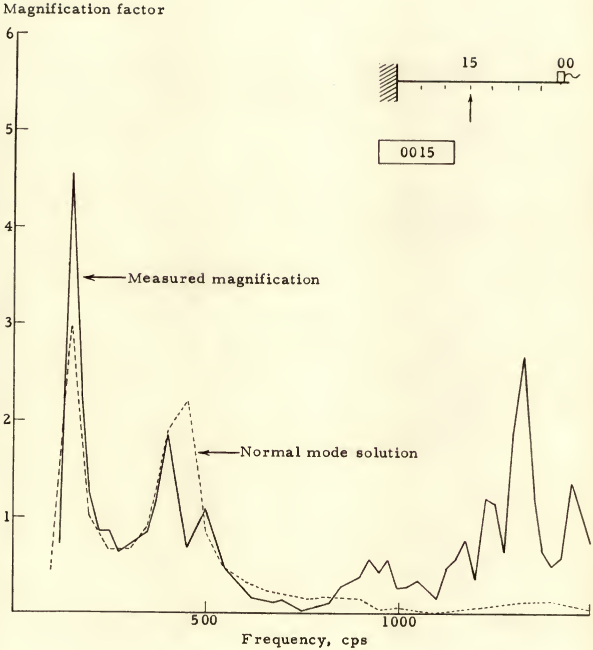

Figure 28. Modulus of Acceleration Transfer Function at 0015

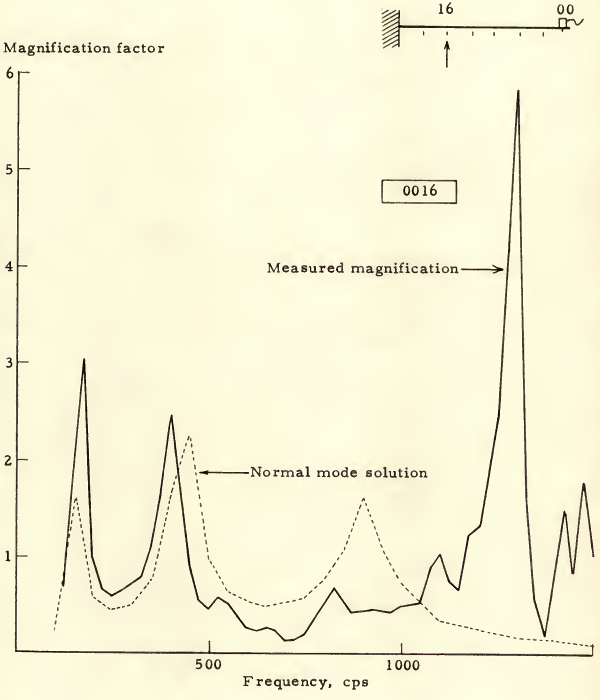

Figure 29. Modulus of Acceleration Transfer Function at 0016

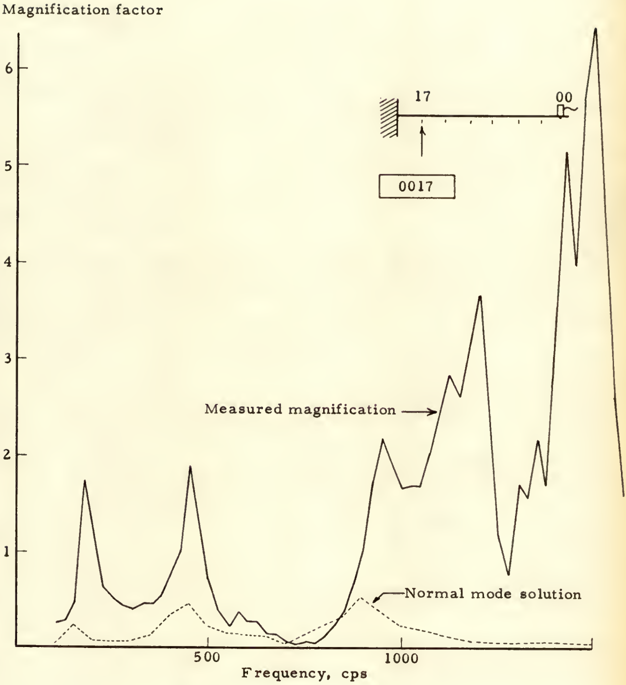

Figure 30. Modulus of Acceleration Transfer Function at 0017

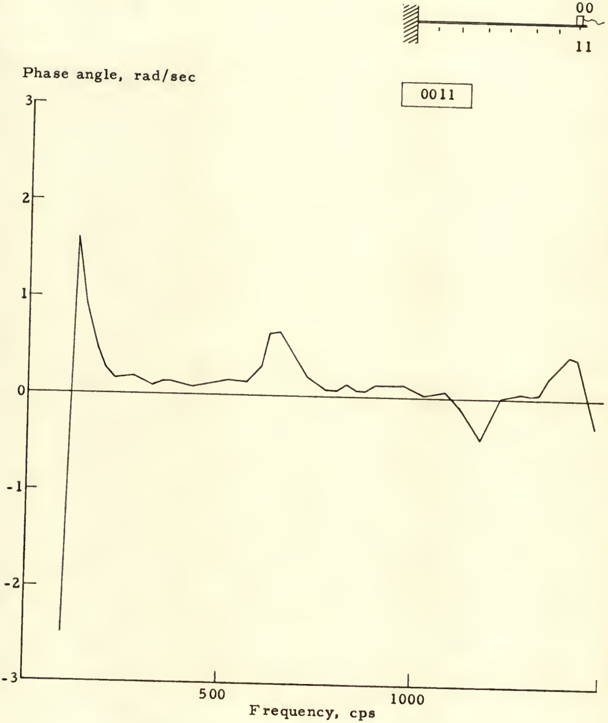

Figure 31. Phase Angle of Acceleration Transfer Function at 0011

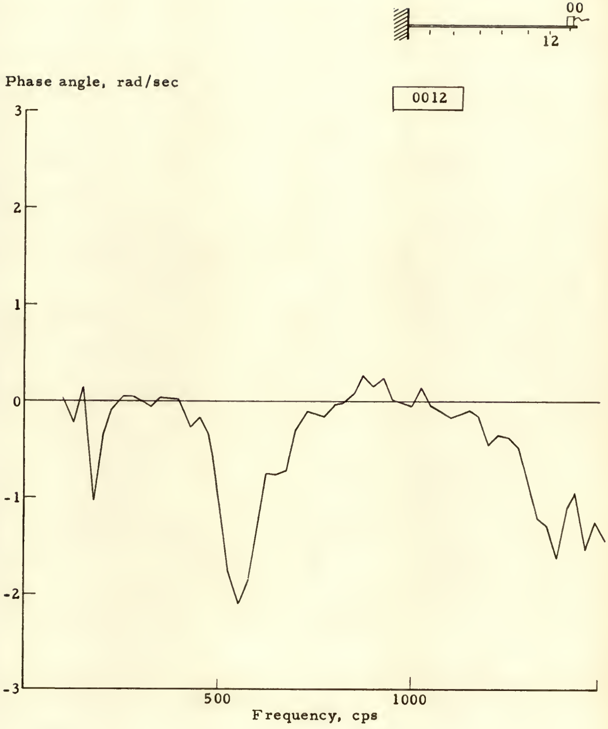

Figure 32. Phase Angle of Acceleration Transfer Function at 0012

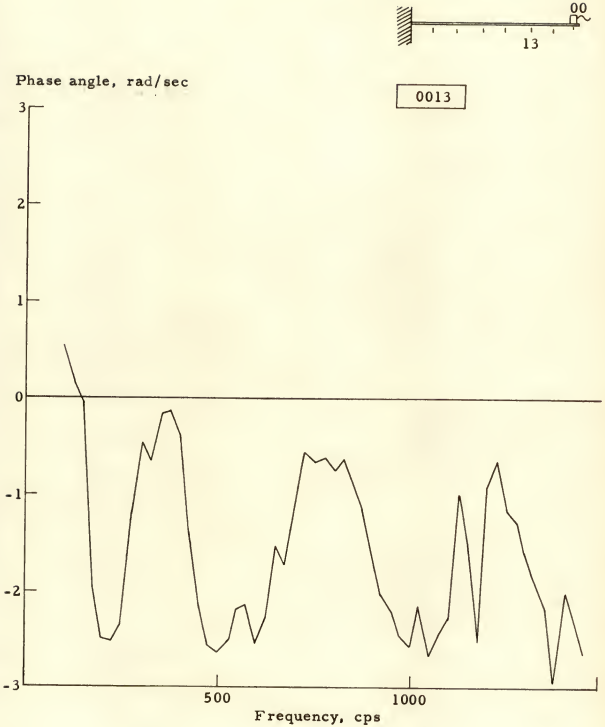

Figure 33. Phase Angle of Acceleration Transfer Function at 0013

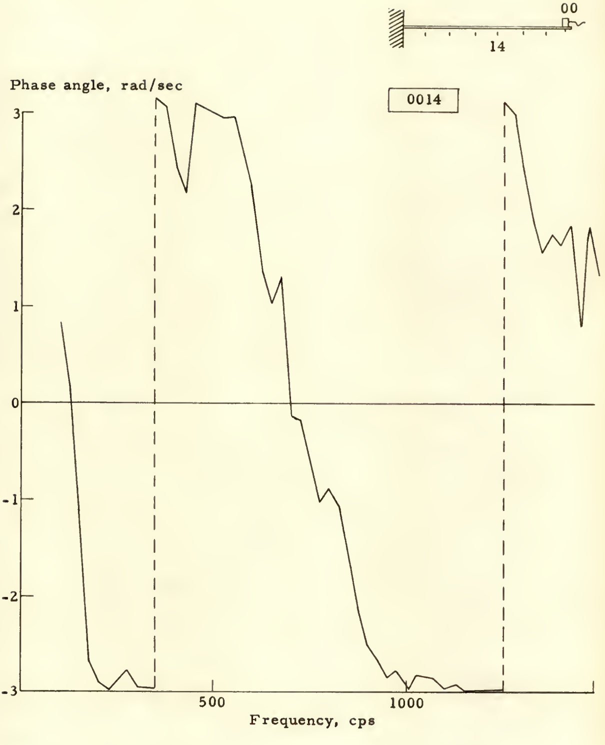

Figure 34. Phase Angle of Acceleration Transfer Function at 0014

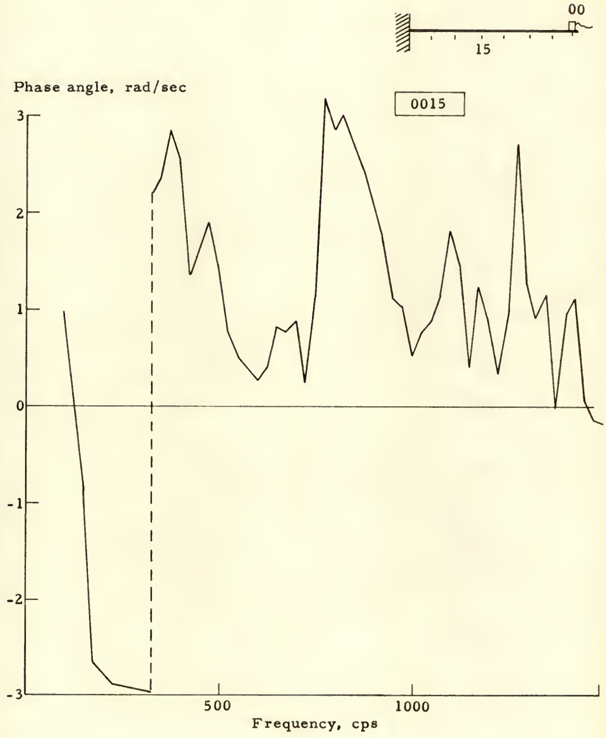

Figure 35. Phase Angle of Acceleration Transfer Function at 0015

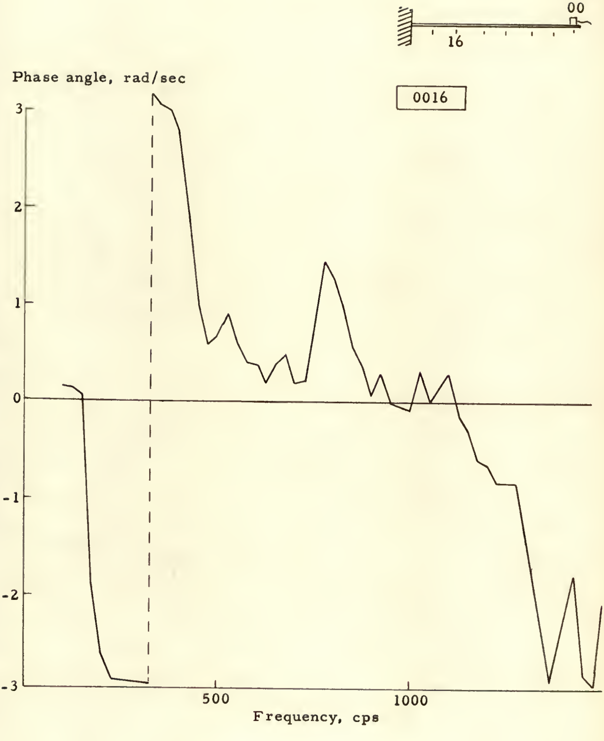

Figure 36. Phase Angle of Acceleration Transfer Function at 0016

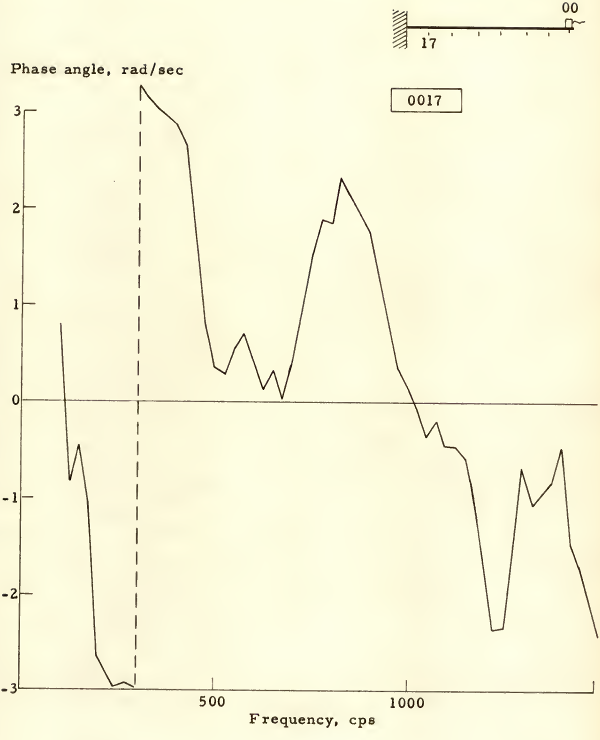

Figure 37. Phase Angle of Acceleration Transfer Function at 0017

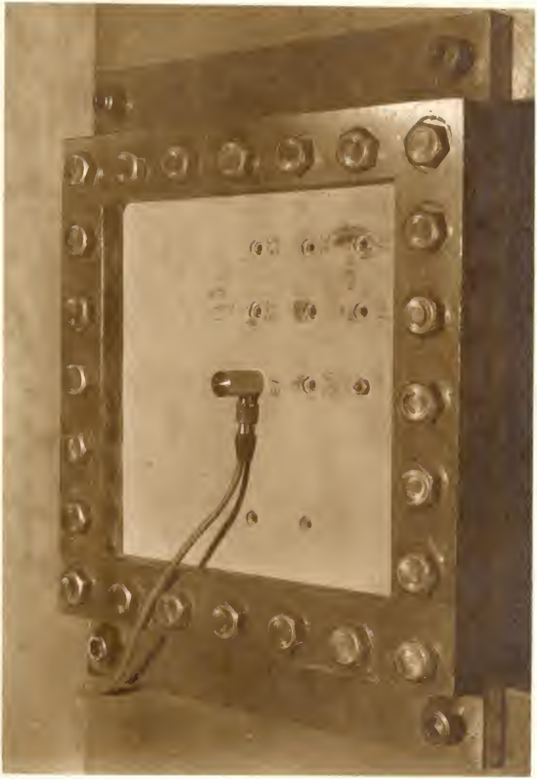

Figure 38. Plan View of Plate

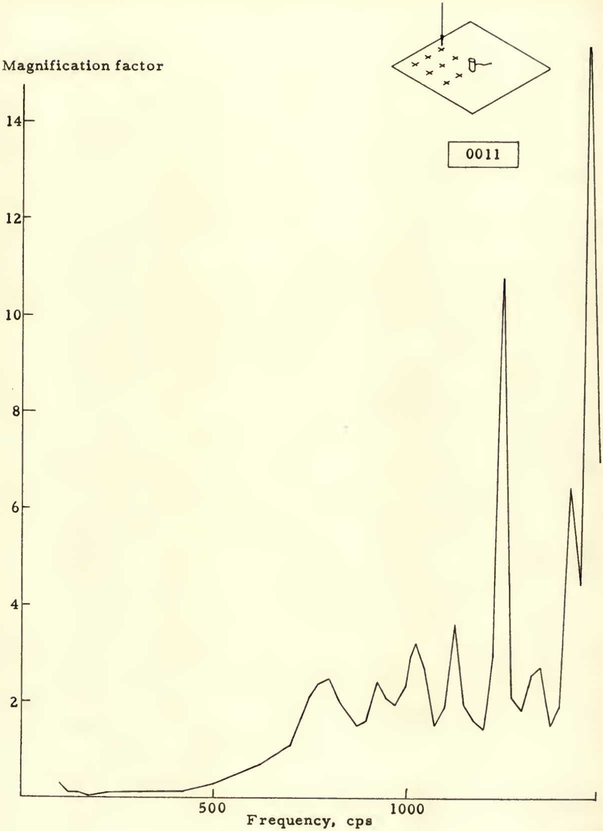

Figure 39. Modulus of Acceleration Transfer Function at 0011

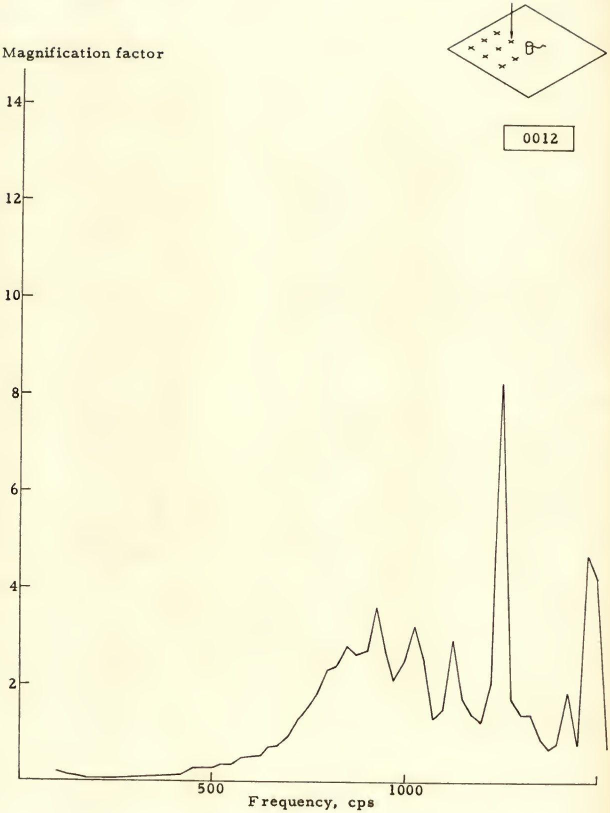

Figure 40. Modulus of Acceleration Transfer Function at 0012

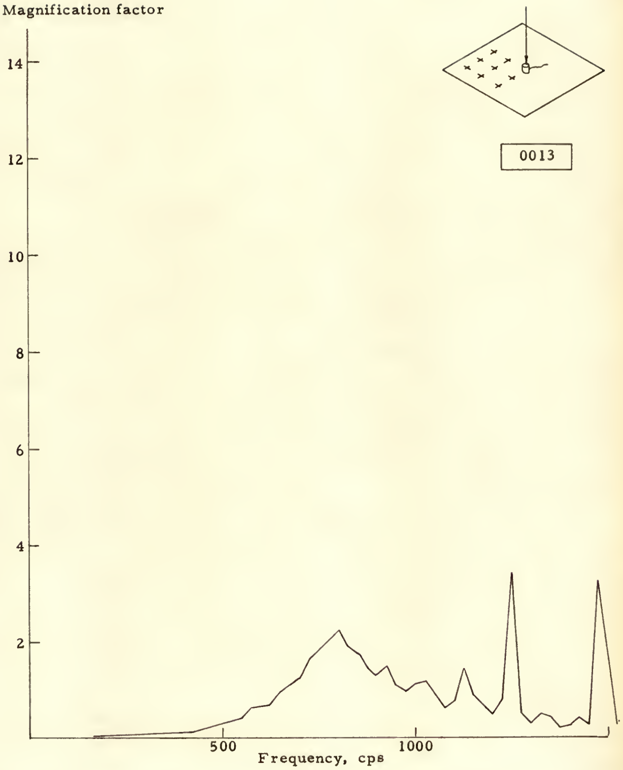

Figure 41. Modulus of Acceleration Transfer Function at 0013

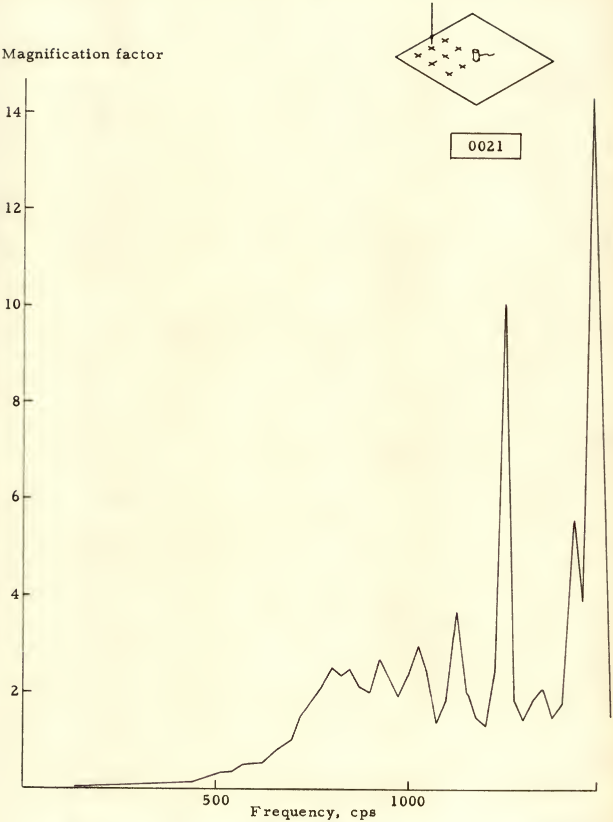

Figure 42. Modulus of Acceleration Transfer Function at 0021

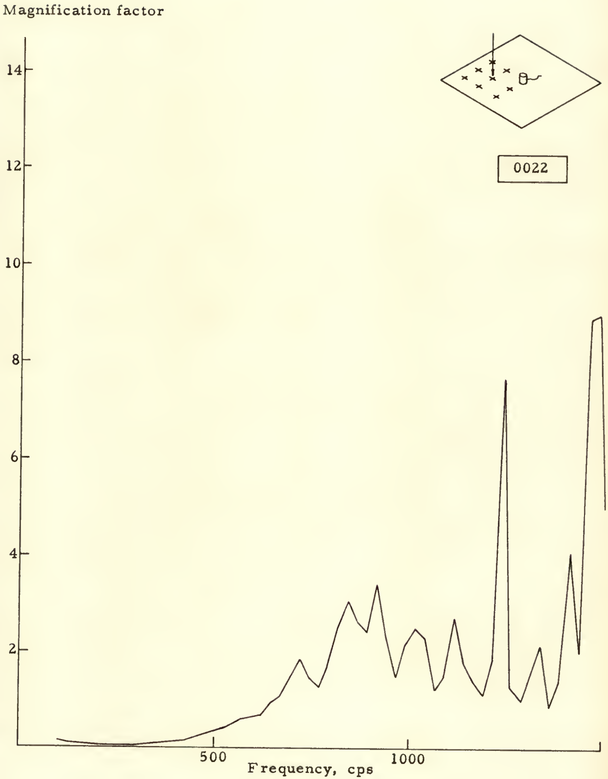

Figure 43. Modulus of Acceleration Transfer Function at 0022

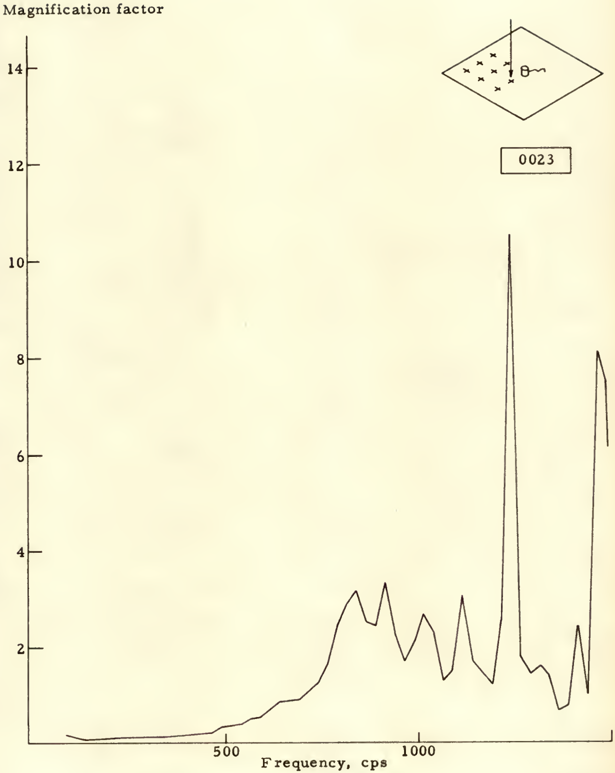

Figure 44. Modulus of Acceleration Transfer Function at 0023

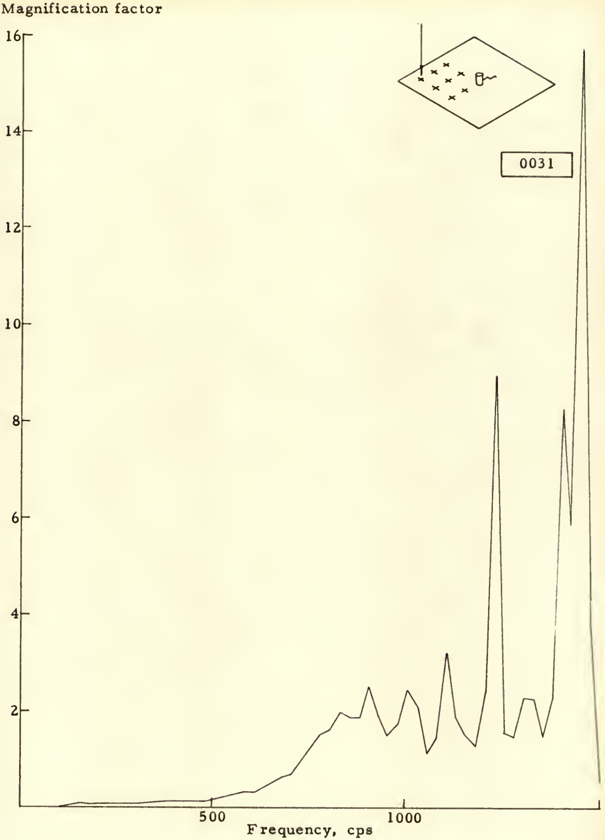

Figure 45. Modulus of Acceleration Transfer Function at 0031

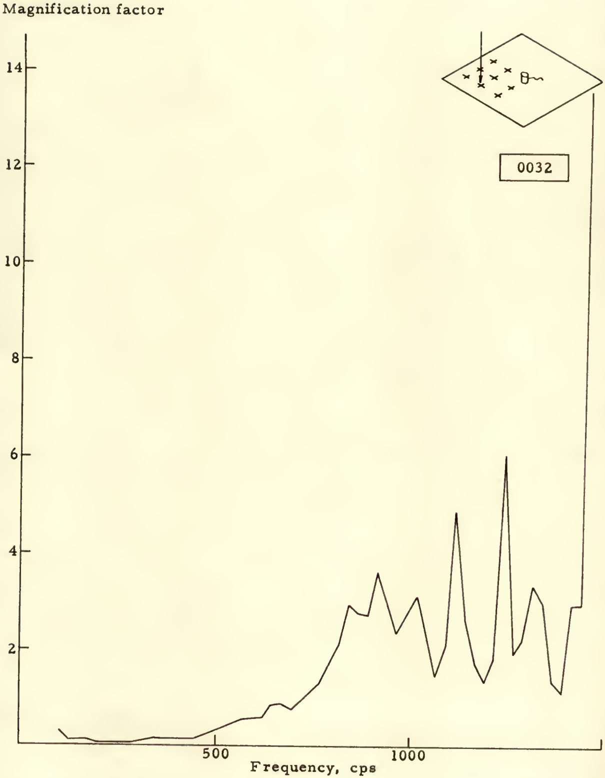

Figure 46. Modulus of Acceleration Transfer Function at 0032

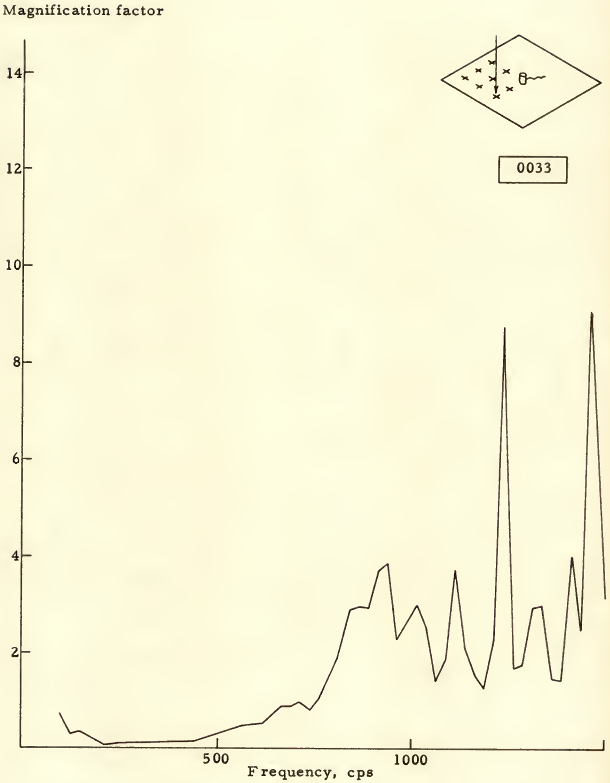

Figure 47. Modulus of Acceleration Transfer Function at 0033

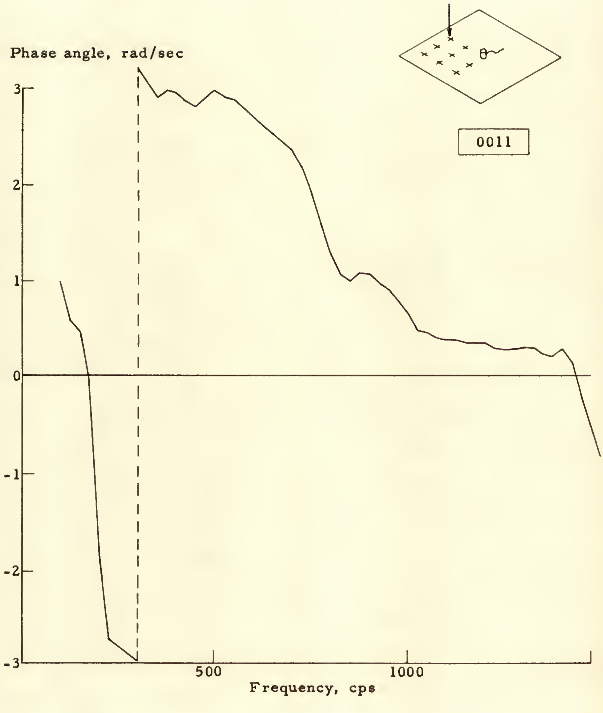

Figure 48. Phase Angle of Acceleration Transfer Function at 0011

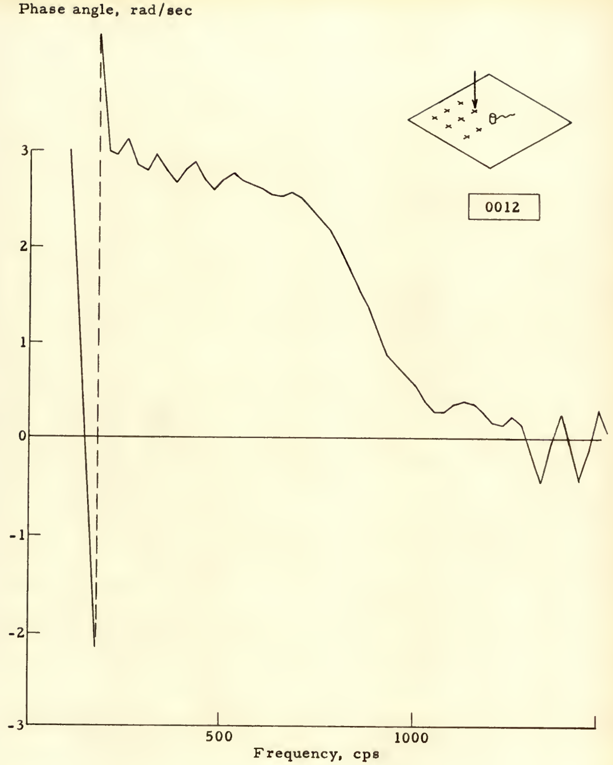

Figure 49. Phase Angle of Acceleration Transfer Function at 0012

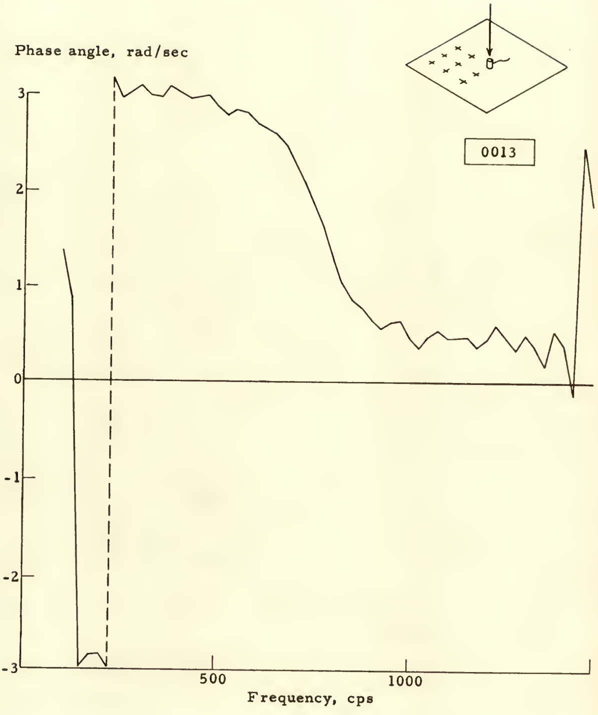

Figure 50. Phase Angle of Acceleration Transfer Function at 0013

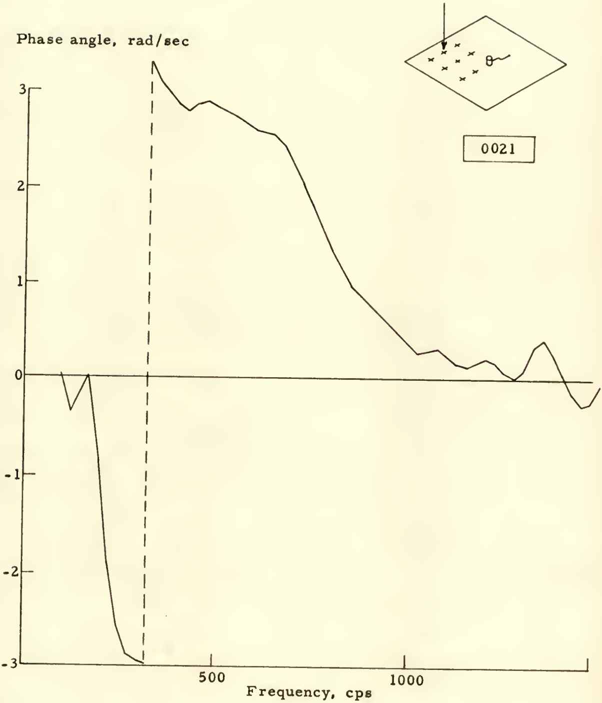

Figure 51. Phase Angle of Acceleration Transfer Function at 0021

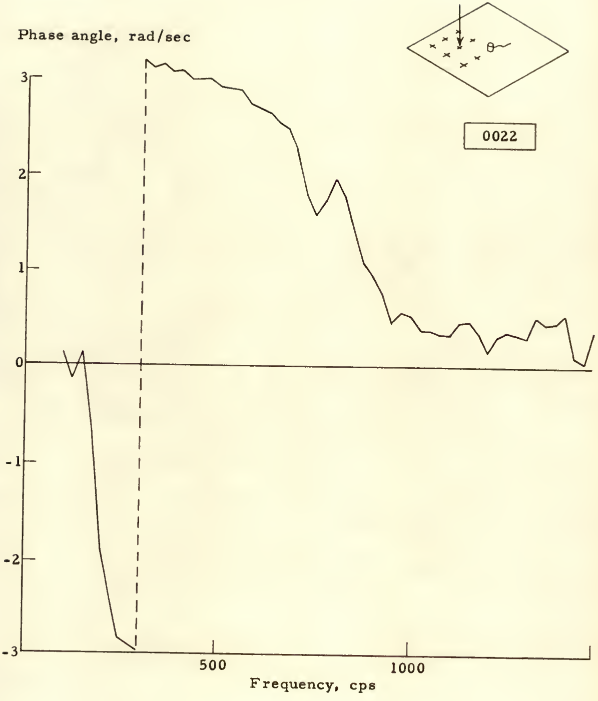

Figure 52. Phase Angle of Acceleration Transfer Function at 0022

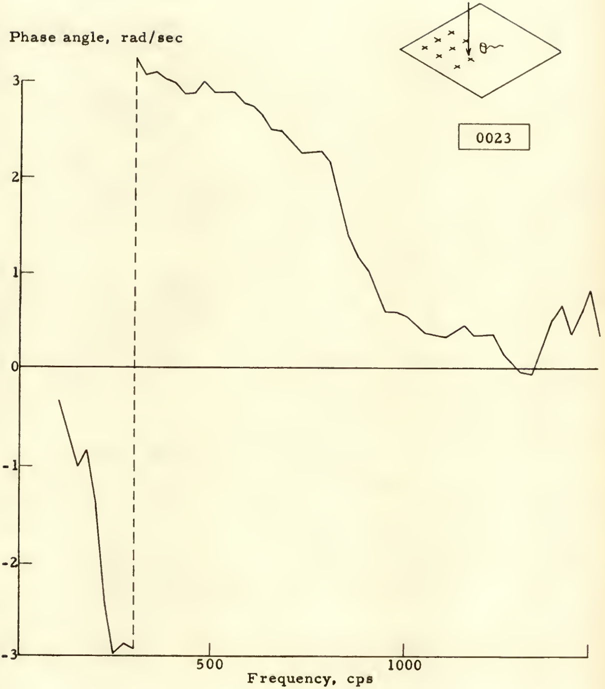

Figure 53. Phase Angle of Acceleration Transfer Function at 0023

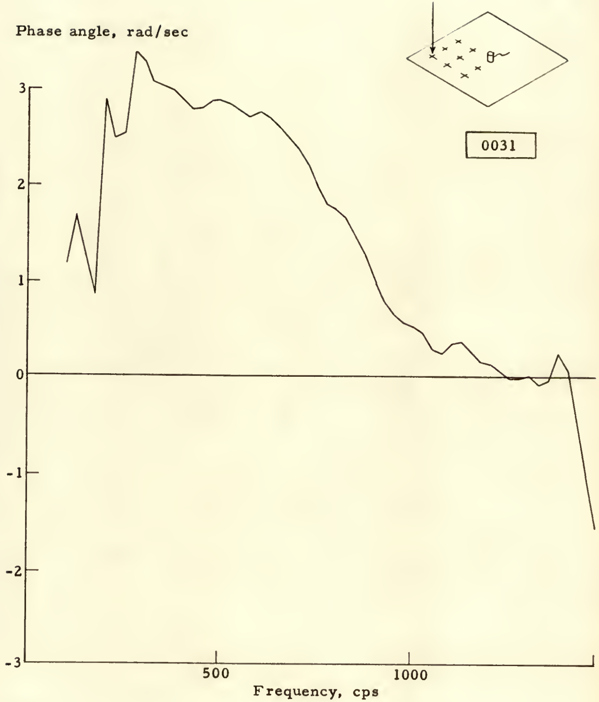

Figure 54. Phase Angle of Acceleration Transfer Function at 0031

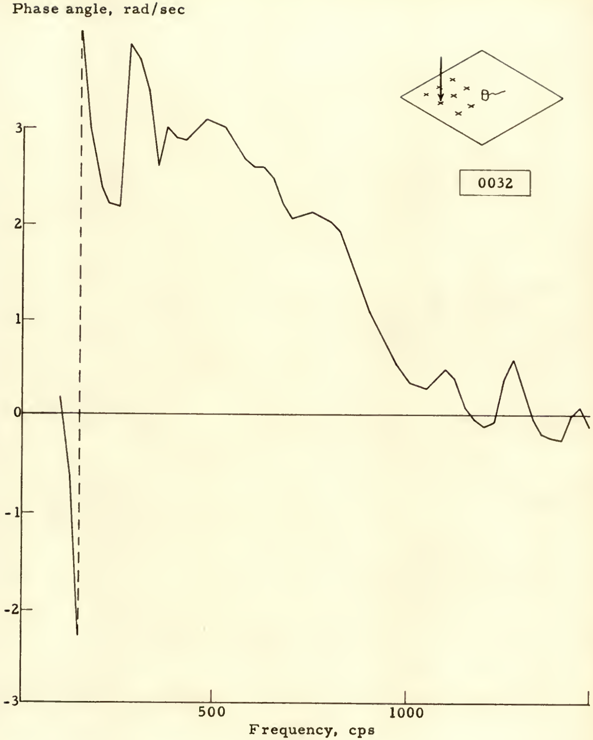

Figure 55. Phase Angle of Acceleration Transfer Function at 0032

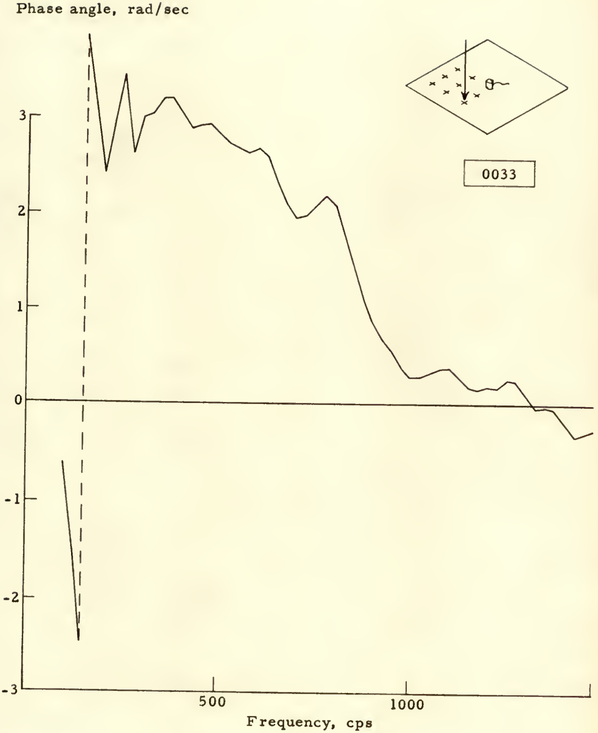

Figure 56. Phase Angle of Acceleration Transfer Function at 0033

An experimental study of plates for determination of their transfer function is much more difficult than would be expected. Because of the large number of modes in which it can vibrate, the plate exhibits a very small driving point impedance. Consequently, the mass impedance of the coil and accelerometer have an appreciable effect on the measurements. The transfer function for the higher frequencies is therefore questionable. In evaluating the transfer function for points other than the center, it will be necessary to drive the plate over its entire surface. The same techniques as before are involved, but the labor is greatly increased. For the center of the plate, the change in the transfer function as a function of space is most easily seen through variation of its phase. With increasing distance from the center of the plate, the space-phase deviations between the various modes become greater. The magnitude of the transfer function remains relatively constant with distance from the center. Since the damping is quite small, the system is likely to vibrate with the same amplitude all over its area. If the damping were larger, the space-amplitude part of the transfer function would decrease very rapidly with the distance from the center of the plate.

Studies of random vibrations of continuous structures have been carried out for distributed stationary excitation, uncorrelated in both space and time. Thomson and Barton [4] indicate the solution for beams when the excitation is confined to a single point. The present study allows one to consider spacewise correlated excitation. Once the transfer function is evaluated for the desired points of interest, the response to any correlated loading can be determined. The transfer functions remain valid for the case of a nonhomogeneous load field and can be used to evaluate the response as long as the system is linear. The cross-correlation technique for measuring $H(r,\omega)$ has the advantage that one can make measurements when the system is in normal operation under service loads. This is clearly an advantage since one does not have to excite the structure with special types of forces to obtain the structure's transfer function, as is done in the case of conventional sinusoidal testing.

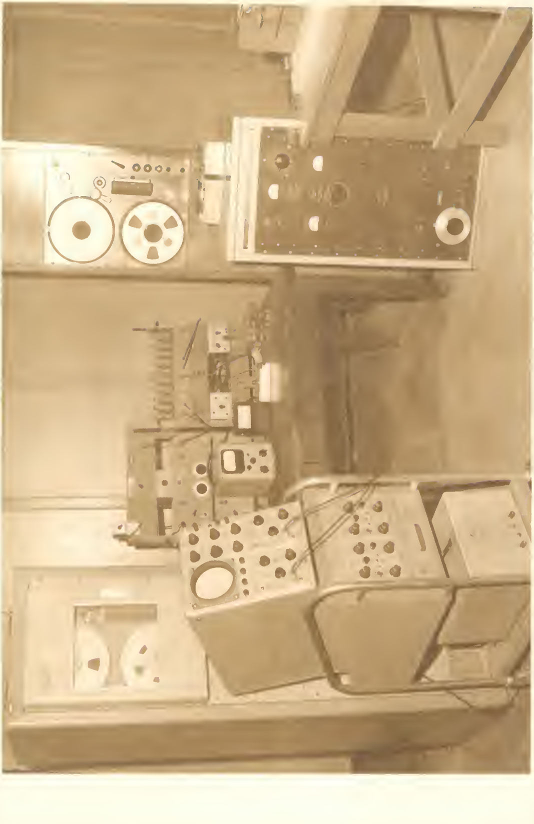

Figure 57. Complete Assembly of Experimental Equipment

LIST OF REFERENCES

1. Bendat, J. B. *Principle and Application of Random Noise Theory*. John Wiley and Sons, New York, 1958.

2. Wax, N. *Selected Papers on Noise and Stochastic Processes*. Dover Publications, New York, 1954.

3. Eringen, A. C. "Response of Beams and Plates to Random Loads." *Journal of Applied Mechanics*, *Transactions of the ASME*, New York, 1957.

4. Thompson, W. T., and Barton, M. V. "The Response of Mechanical Systems to Random Excitation." *Journal of Applied Mechanics*, Vol. 79, 1957, p. 248.

5. Rice, S. O. "Mathematical Analysis of Random Noise." *Bell Systems Technical Journal*, Vol. 23, 1944, pp. 282-332; Vol. 24, 1945, pp. 46-156.

6. Booton, R. C. *Proceedings of Symposium on Nonlinear Circuit Analysis*. Brooklyn Polytechnic Institute, 1953.

7. Nash, W. A. "Response of an Elastic Plate to a Distributed Random Pressure Characterized by a Separable Cross-Correlation." Technical Note No. 1, AFOSR, ~~1959.~~ 1961

8. Lee, Y. W. *Statistical Theory of Communication*. John Wiley and Sons, Inc., New York, 1960.

9. Trubert, M., Kizner, G., and Nash, W. A. "Experimental Determination of a Statistical Representation of the Noise Field of a Subsonic Air Jet." *Developments in Mechanics*, *Proceedings of the Seventh Midwestern Mechanics Conference*, *Vol. I*, Plenum Press, New York, 1961.

10. Young, D., and Felgar, R. P., Jr. "Table of Characteristic Functions Representing Normal Modes of a Beam." University of Texas Publication No. 4913, July 1, 1949.

Additional Readings

Beer, F. P. "On the Response of Linear Systems to Time Dependent, Multidimensional Loadings." Journal of Applied Mechanics, Transactions of the ASME, Vol. 83, New York, 1961.

Blackman, R. B., and Tuckey, J. W. "Measurements of Power Spectra from the Viewpoint of Communication Engineering." Bell Systems Technical Memorandum, January-March, 1958.

Chuang, K., and Kazda, L. F. "A Study of Nonlinear Systems with Random Inputs." AIEE Transactions, Part II, Vol. 78, 1959.

Clarkson, B. L. "Correlation of Pressure Around a Jet Engine." WADC Technical Report No. 59-676, University of Minnesota Conference on Acoustical Fatigue, March, 1961, p. 85.

Crandall, S. H. Random Vibration. The Technology Press, Cambridge, Mass., 1958.

Davenport, W. B. An Introduction to the Theory of Random Signals and Noise. McGraw-Hill Book Company, New York, 1958.

Harrison, M. "Pressure Fluctuations on the Wall Adjacent to a Turbulent Boundary Layer." Department of the Navy, David Taylor Model Basin, Report 1260, December, 1958.

Lebedev, V. L. Random Processes in Electrical and Mechanical Systems. The State Publishing House of Physical and Mathematical Literature, Moscow, 1958.

Lyon, R. H. "Response of Strings to Random Noise Fields." Journal of the Acoustical Society of America, New York, 1956.

Middleton, D. Introduction to Statistical Communication Theory. McGraw-Hill Book Company, New York, 1960.

Samuels, J. C. "Response of a Simply Supported Timoshenko Beam to a Purely Random Gaussian Process." Journal of Applied Mechanics, Transactions of the ASME, Vol. 80, New York, 1958.

BIOGRAPHICAL SKETCH

Harold George Kizner was born January 14, 1936, in Brooklyn, New York. He attended Virginia Polytechnic Institute and was graduated with the degree of Bachelor of Science in Engineering in June, 1956. He received the Master of Science degree from Massachusetts Institute of Technology in February, 1958. From September, 1958, to August, 1960, he was associated with the Lockheed Missile Systems Division in Sunnyvale, California, while attending Stanford University.

In September, 1960, George Kizner joined the University of Florida faculty as a Research Associate to undertake studies leading to a Ph. D. in Engineering Mechanics. While at the University, he co-authored several technical publications.

This dissertation was prepared under the direction of the chairman of the candidate's supervisory committee and has been approved by all members of that committee. It was submitted to the Dean of the College of Engineering and to the Graduate Council, and was approved as partial fulfillment of the requirements for the degree of Doctor of Philosophy.

June, 1962

Joseph Weil
Dean, College of Engineering

Dean, Graduate School

Supervisory Committee:

William A. Nash
Chairman

T. C. Huang

William L Sawyer

F S George

C. B. Smith